

1 **Failure mode of rainfall-induced landslide of granite residual soil, southeastern**
2 **Guangxi province, China**

3 **Shanbai Wu^{1, 2, 3, 4}, Ruihua Zhao^{1, 2, 3}, Liping Liao^{1, 2, 3*}, Yunchuan Yang^{1, 2, 3*}, Yao Wei^{1, 2, 3}, Wenzhi Wei^{1, 2, 3}**

4 ¹College of Civil Engineering and Architecture, Guangxi University, Nanning 530004, China;

5 ²Guangxi Key Laboratory of Disaster Prevention and Engineering Safety, Guangxi University, Nanning 530004, China;

6 ³Key Laboratory of Disaster Prevention and Structural Safety of Ministry of Education, Guangxi University, Nanning 530004, China;

7 ⁴Faculty of Engineering, China University of Geosciences, Wuhan 430074, China

8 **Correspondence:** Liping Liao (011lp@163.com), Yunchuan Yang (yyunchuan@163.com)

9
10 **Abstract.** Granite residual soil landslides are widely distributed in the southeast of Guangxi, China.
11 They are posing threats to local communities, economic development, and ecological restoration. To
12 understand the failure mode of the landslide can provide a scientific basis for early warning and
13 prevention. In this study, it conducted artificial flume model tests to investigate the failure mode of
14 granite residual soil landslide. The macroscopic phenomena of landslides were observed and
15 summarized. The response and variations of soil moisture content and pore water pressure were
16 analyzed. And the discrepancies in landslide initiation were explored. The results had three aspects.
17 (1) The response of volume moisture content was not synchronized with that of pore water pressure.
18 Their variations were influenced by initial dry density, slope angle, and rainfall intensity. The
19 fluctuation of pore water pressure depended on soil mechanical behavior and its diffusion. (2) The
20 differences in the formation process of granite residual soil landslides included the initiation time and
21 mode. The starting time of landslide was delayed with increasing initial dry density and slope angle,
22 but shortened with increasing rainfall intensity. The failure mode could be changed from a sudden
23 type to a progressive type due to the increase in initial dry density. (3) There are five stages in the
24 landslide mobilization as follows: rain infiltration and crack generation, soil slide at the slope toe,
25 occurrence of surface runoff and soil erosion, formation of steep-free surface, and soil slide at the
26 upper slope. This research can provide valuable reference for the prevention and early warning of
27 granite residual soil landslide in southeastern Guangxi.

28
29 **Keywords:** Granite residual soil; Rainfall-induced landslide; Failure mode; Flume model test;
30 Southeastern Guangxi

33 1 Introduction

34 Rainfall-induced landslides are the most common geohazards in the tropical and subtropical areas
35 covered by granite residual soil, such as Brazil (Lacerda, 2007; Coutinho et al., 2019), Singapore
36 (Rezaur et al., 2003; Rahardjo et al., 2008; Rahardjo et al., 2012; Zhai et al., 2016; Zhang et al.,
37 2019), Malaysia (Rahman et al., 2018), Korea (Kim et al., 2004; Pham et al., 2019), the southern
38 (Jiao et al., 2005; Fan et al., 2018; Luo et al., 2021; Liu et al., 2021; Liu et al., 2020a; Liu et al.,
39 2020b) and southeastern China (Xia et al., 2019; Yao et al., 2021; Shu et al., 2021; Zhao et al., 2021).
40 Guangxi is located in southeastern China, where granite is concentrated in the southeast, and
41 landslides occur frequently (Liao et al., 2019). Hot and rainy climatic conditions have caused strong
42 weathering of the surface granite, giving birth to tens of thousands of residual soil. This provides a
43 superior environment for the formation of landslides. Therefore, the southeastern Guangxi has been
44 threatened by granite residual soil landslides for a long time. Granite residual soil is a regional
45 special soil (Ministry of Construction of the People's Republic of China, 2002). One reason is that it
46 has the dual mechanical properties of cohesive soil and sandy soil. The other is that it exhibits an
47 abnormal combination of poor physical properties, such as high liquid limit and large void ratio, and
48 high-strength properties in a natural state (Chen et al., 2011). However, granite residual soil is
49 extremely sensitive to rainfall. It is easy to disintegrate and soften, and induce a wide range of
50 landslides (Dahal et al., 2008; Liu et al., 2020a; Zhang and Tang, 2013). Although shallow landslides
51 are the main type (Rahardjo et al., 2008; Kim et al., 2004), they still have the characteristics of high
52 frequency (Kim et al., 2015), suddenness and mass occurrence.

53 The failure mode of residual soil landslide is an important basis for landslide monitoring and early
54 warning (Rezaur et al., 2003). In this regard, many scholars have conducted in-depth studies on
55 granite residual soil landslide and other residual soil landslide through statistical analysis, model tests
56 and numerical simulations. They classified the type of granite residual soil (Wu, 2006b) and studied
57 on the physical mechanical properties (Zhu and Anderson, 1998; Chen et al., 2011; Zhang and Tang,
58 2013; Chen and Gong, 2014; Xia et al., 2019), engineering characteristic (Wu, 2006a; Xu et al., 2017)
59 and microstructure (Li et al., 2017; Wang et al., 2018). The formation condition (Zhan et al., 2012;
60 Zuo et al., 2015) and instability mode (Zhao and Hu, 2005; Dahal et al., 2008; Xu and Jian, 2017) of
61 granite residual soil landslides were revealed. They found and confirmed that the failure mode of
62 residual soil slope is different from that of homogeneous soil - rock slope. This is because it includes
63 arc slip, plane slip and front shear slip, but plane slip is dominant (Fu et al., 2018). The failure
64 surface is parallel to the original slope (Kim et al., 2004). They also pointed out rainfall is the most
65 important external triggering factor due to two aspects (Coutinho et al., 2019). One is the deepening
66 of the wetting peak induced by rainfall infiltration (Kim et al., 2004). Second, the increase in soil
67 water content and pore water pressure can lead to a decrease in slope stability (Gasmo et al., 2000;
68 Rezaur et al., 2003; Rahardjo et al., 2005; Lacerda, 2007; Rahardjo et al., 2008). Thus, in the process
69 of landslide formation, the variation of physical property parameters such as moisture, matric suction
70 or pore pressure play an important role in the residual soil landslide (Kassim et al., 2012; Igwe and
71 Fukuoka, 2014; Pham et al., 2019; Zhai et al., 2016). Rainfall triggered mechanisms focus on
72 completely weathered granite fill slope in Hong Kong, China. They are static liquefaction (Chen et
73 al., 2004) and the transition from slide to flow due to localized transient pore water pressure (Take et

74 al., 2004). However, static liquefaction is impossible due to unsaturated condition. Instead, local
75 transient pore water pressure can induce the initially slip, which further triggers the high-speed slide
76 (Take et al., 2004). Another finding is that the initial dry density (Mukhlisin et al., 2008) and slope
77 angle (Liu et al., 2020a; Liu et al., 2020b) can affect the water permeability and control the formation
78 of landslides (Xu et al., 2018). Many scholars have carried out related studies on the relationship
79 between dry density of other types of soil, such as sandy soil, volcanic residual soil, and gravel soil,
80 and the initiation of landslides. They found through model tests that the initial density can determine
81 the stress-strain characteristics of the soil, and it corresponds to the initiation mechanism of dilation
82 and contraction (Dai et al., 1999a; Dai et al., 1999b; Mckenna et al., 2011). The macroscopic
83 phenomena corresponding to these two mechanisms are that the saturated loose slope will suddenly
84 liquefy and flow rapidly, while the saturated dense slope will slowly creep (Iverson et al., 2000). It
85 can be seen that there is a significant difference in the sliding motion rate of sand landslides (Iverson,
86 2005). Especially when the dry density is optimal, the moving speed and sliding distance of the
87 landslide are both maximums (Wang and Sassa, 2001). This is mainly because the initial dry density
88 affects the soil-water interaction and soil permeability (Ng and Pang, 2000; Jiang et al., 2017). For
89 example, high-density steep slopes are much more resistant to rainwater penetration than low-density
90 gentle slopes (Xu et al., 2018). A gentle slope can lead to better accumulation of rainwater, a faster
91 increase in water content, but a slower rate of soil collapse (Liu et al., 2020a; Liu et al., 2020b).
92 Other scholars have further confirmed the above results through numerical simulations. That is, the
93 initial dry density has a decisive influence on the movement accumulation and evolution process of
94 the landslide. It is mainly reflected in the significant differences in slip rate (Liang et al., 2017).

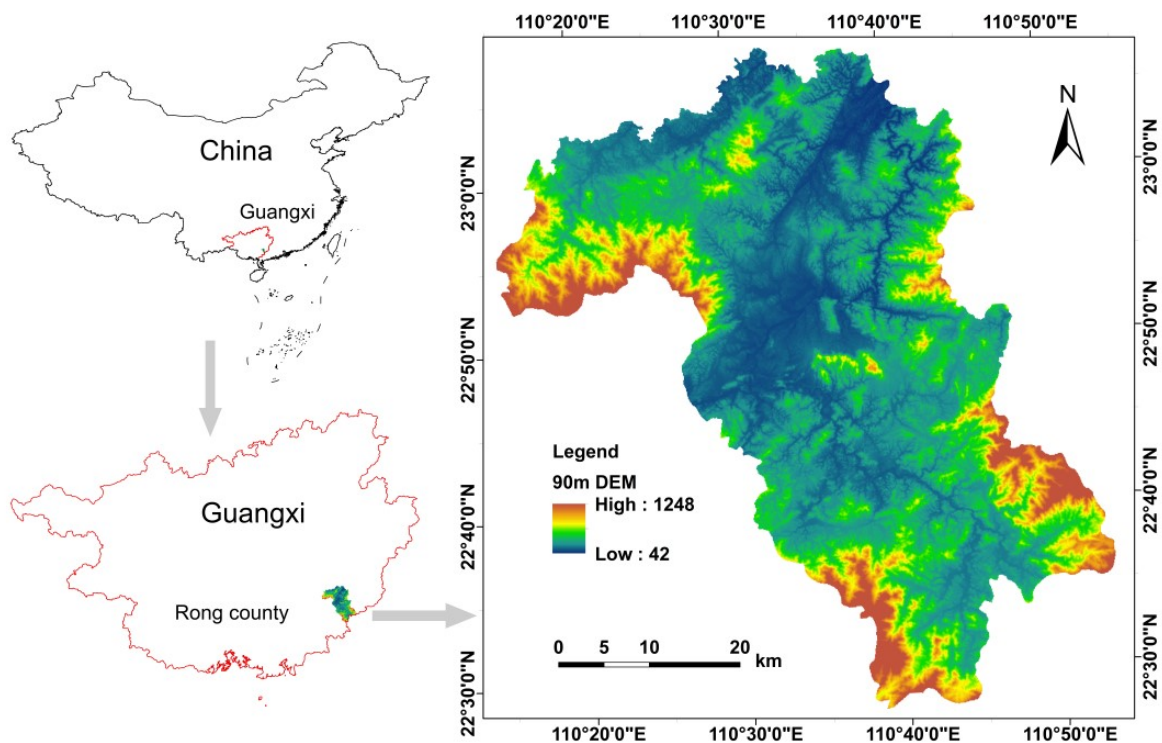
95 The above researches have pointed out the direction for the follow-up work. However, most of the
96 conclusions related to failure process focus on gravel soil (Chen et al., 2017; Liao et al., 2018; Wu et
97 al., 2019), sandy soil (Moriwaki et al., 2004; Huang et al., 2008; Huang and Yuin, 2010), fill slope
98 (Chen et al., 2004; Take et al., 2004), clay soil (Elkamhawy et al., 2018; Miao et al., 2022) and loess
99 slope (Tu et al., 2009; Zou et al., 2020). Moreover, the degree of development of granite weathering
100 crust is closely related to the climate, topography and environment (Qu et al., 2000). The granite
101 residual soil has significant heterogeneity characteristics in terms of thickness, physical and
102 mechanical property (Rahardjo et al., 2002; Rahardjo et al., 2012). These special characteristics lead
103 to the complex initiation modes of landslides (Calcaterra and Parise, 2005; Mukhlisin and Taha, 2012;
104 Liu et al., 2020a; Xia et al., 2019). At present, the failure mode of granite residual soil slope in the
105 southeast of Guangxi has not been studied, which has brought challenges to the prevention and early
106 warning of landslides. Therefore, some scientific issues need to be solved. For example, what are the
107 similarities and differences of the failure process of granite residual soil slope? How do the physical
108 parameters of residual soil change? In this paper, it conducted artificial flume model tests to resolve
109 the above issues. Firstly, the macroscopic phenomena of landslide is observed and summarized.
110 Subsequently, the variation characteristics of soil moisture content and pore water pressure are
111 analyzed. Finally, the differences in the initiation of rainfall-induced landslide are discussed.

112

113 **2 Field site and method**

114 **2.1 Field site**

115 Rong County is a typical high-prone area of rainfall-induced landslide of granite residual soil in
116 southeast Guangxi (Liao et al., 2019). It is located between longitude 110°15'00"-110°53'00" E and
117 latitude 22°27'00"-23°07'00" N (Fig. 1). The county covers an area of 2257 km², with an average
118 annual rainfall 1737.4 mm a⁻¹. The rainy period is from April to September, and the rainfall in this
119 period accounts for 78.6 % of the average annual rainfall. The area of magmatic rocks is 1260.09
120 km², accounting for 55.83 % of the total area of the county. The lithology is mainly granite with an
121 area 1219.06 km².

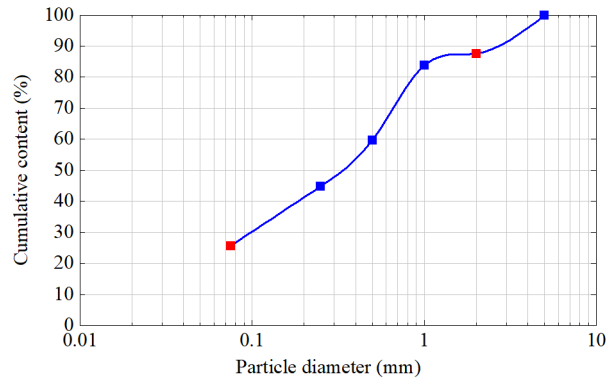


122
123 Figure 1. Study area.

124
125 **2.2 Method**

126 Longtou village in Liuwang town is a landslide high-prone area in Rong County. Therefore, the test
127 soil comes from Longtou village. Specific gravity of the soil is 2.71, and the minimum and maximum
128 of dry density are 1.18 g cm⁻³ and 1.72 g cm⁻³. Particle data is the average of three sets of sieve tests
129 on granite residual soil (Fig. 2). The red grid points in Figure 2 represent the cumulative content of
130 gravel (diameter < 2 mm) and silt and clay (diameter ≤ 0.075 mm). They are 87.52 % and 25.62 %.
131 The angles of natural slope in the study area are 30 ° - 45 ° and mainly 40 ° - 45 °. The dry density of
132 superficial soil is 1.20 - 1.40 g cm⁻³. The average mass moisture content is 6 %-10 % (Wen, 2015).
133 Only two initial dry densities of 1.20 g cm⁻³ and 1.40 g cm⁻³ are set to highlight the discrepancies
134 between tests (Table 1). Two slope angles of 40 ° and 45 ° are established. Initial mass moisture
135 content is controlled in the range of 6 % to 10 %. Heavy rainfall is the main factor in the formation
136 of landslides (Wei et al., 2017). Hence, rainfall intensity and duration are set based on rainfall data

137 from multiple landslide events in the study area in 2010 (Wen, 2015). There are 1-3 periods of
 138 rainfall, and each period lasts for 8 hours with an interval of 15 hours. Rainfall intensities are 60 mm
 139 h⁻¹ and 90 mm h⁻¹ respectively. Furthermore, the groundwater level in the study area is relatively deep.
 140 The landslide initiation of granite residual soil does not depend on the fluctuation of groundwater
 141 level. Therefore, the groundwater level is not considered in the tests.



142
 143 Figure 2. Particle gradation of granite residual soil.

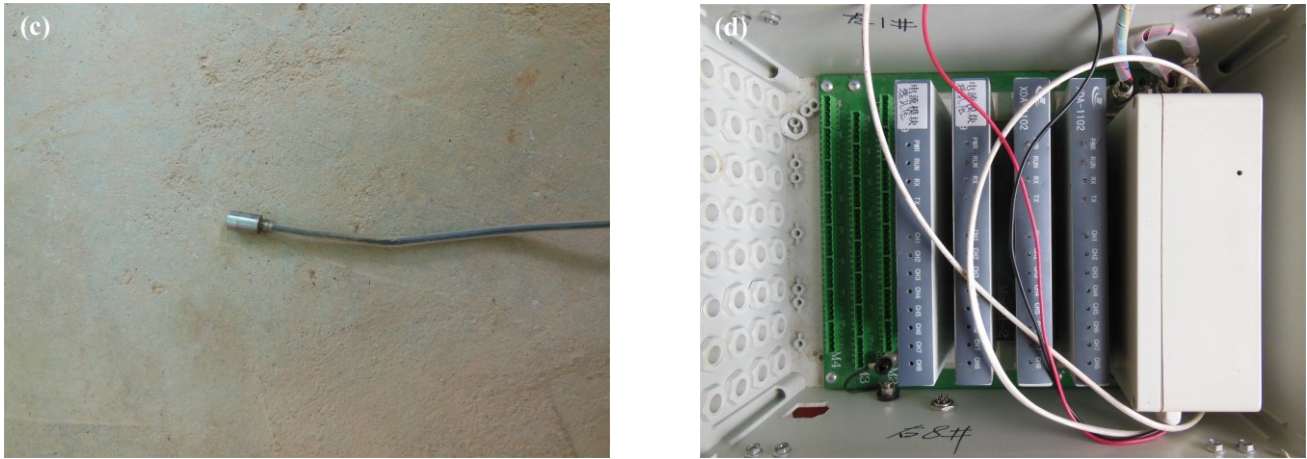
144
 145 Table 1. Scheme of artificial flume model tests.

Test number	Slope angle (°)	Initial dry density (g cm ⁻³)	Rainfall intensity (mm h ⁻¹)	Rainfall duration (h)
1	45	1.20	60	8, 8, 8
2		1.40	60	8, 8, 8
3		1.20	90	8, 8
4		1.40	90	8, 8
5	40	1.20	60	8, 8, 8
6		1.20	90	8

146
 147 Test equipments are composed of rainfall control system, data testing system, and flume model.
 148 Rainfall control system contains central control system, suction pump, water tank, hose, brace, and
 149 nozzle. The size of water output can be set in the rainfall control system. The distance from the
 150 nozzle to slope crest is 2.3 m. The effective rainfall area of the tests is 6 m², and the rainfall is
 151 calibrated before the formal test. Data testing system consists of sensors and data collectors (Fig. 3).
 152 The minimum time unit for data collection is 1 min, and the storage space of the data collector is
 153 limited. Hence, the acquisition frequency of volume moisture content and pore water pressure is set
 154 to 1 min and 3 min, respectively.

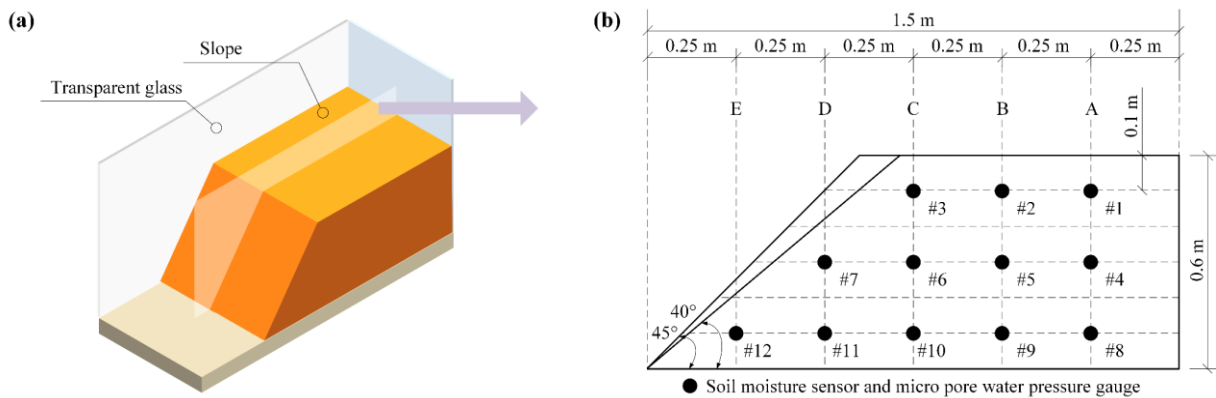


155



156
 157 Figure 3. Testing equipments. (a) Soil moisture sensor (the model is MP-406B). (b) Soil moisture collector (the model is
 158 M-16). (c) Micro gauge of pore water pressure (the model is HC-25). (d) Pore water pressure collector (the model is
 159 MCU).

160
 161 The length, width and height of test slope are 1.5 m, 0.8 m, and 0.6 m, respectively. The slope is
 162 divided into six layers, and the thickness of each layer is 0.1 m (Fig. 4). Firstly, a sufficient amount
 163 of air-dried soils are screened. Secondly, the required water is calculated based on the current and
 164 designed moisture content. Subsequently, this water is sprayed evenly into the soil. When the water
 165 and soil are fully mixed, they are placed in a container and kept for 24 hours. Finally, when moisture
 166 content of the mixture meets the requirement of designed moisture content, the slope model begins to
 167 be made. The accuracy of initial dry density must be guaranteed, so the soil of each layer is
 168 compacted with the wooden hammer. In addition, twelve monitoring points are set up inside the
 169 model. They belong to five positions. Each monitoring point consists of a soil moisture sensor and a
 170 micro gauge of pore water pressure (Fig. 4b).



171
 172 Figure 4. Flume model. (a) Three-dimensional schematic of the model. (b) Center section of the slope and sensor
 173 locations.

174 3 Results

175 3.1 Macroscopic phenomena of tests

176 (1) Test 1

177 During the first rainfall, when the rainfall lasts for 50 min, two small ditches are found on the

178 slope surface. At this time, the soil at the slope toe slips, and triggers the soil on the trailing edge to
179 slide. The instability area is fan-shaped and located at the left side of the slope toe. Its length is three-
180 quarters of the total length of the slope. When the rainfall lasts for 421 min, a new ditch developing
181 on the slope shoulder is connected with the original instability area. In the second rainfall, the ditches
182 are continuously eroded. At the same time, many fine particles are moved to the slope toe by rain.
183 When the rainfall lasts for 559 min, the soil of the left slope shoulder begins to slide, causing the
184 formation of tensile crack at the slope crest. Then the soil around the crack slips and accumulates to
185 the slope toe. During the third rainfall, the continuous soil slide leads to the occurrence of a steep
186 free surface. When the rainfall lasts for 1324 min, the soil of the steep surface starts to slide. The soil
187 sliding does not stop until the slope gradient becomes gentle.

188 (2) Test 2

189 When the first rainfall lasts for 67 min, the soil on the left side of the slope toe begins to slip. The
190 area of sliding range gradually extends. When the rainfall lasts 431 min, the instability range has
191 been extended to the slope shoulder, and the seventh sensor is exposed. Subsequently, the soil on the
192 right side of the slope toe slips, causing the soil slide in the middle slope. During the second rainfall,
193 tiny cracks are found on the right side of slope. When the rainfall lasts for 524 min, the soil around
194 the crack slips, and the sliding surface is arc-shaped. Owing to continuous rainfall, the process of soil
195 slide occurs repeatedly, and the gullies forms. The slope surface is eroded by third rainfall. The ditch
196 on the right side of slope extends and the slope eventually stabilizes.

197 (3) Test 3

198 In the first rainfall process, when the rainfall lasts for 32 min, tensile cracks appear successively
199 on the slope toe, and the soil around the cracks slips (Fig. 5a). Subsequently, a steep free surface is
200 formed. When the rainfall lasts for 39 min, the soil in the middle slope begins to slide (Fig. 5b).
201 When the rainfall lasts for 215 min, the soil on the slope shoulder starts to slip due to unbalance
202 internal forces (Fig. 5c). It causes the sensor #3 to deviate from the embedded position. When the
203 second rainfall lasts for 811 min, blocky soil slides suddenly on the right slope toe (Fig. 5d). When
204 the rainfall lasts for 923 min, massive soil on the right slope shoulder begins to slides owing to the
205 unloading effect of the slope toe (Fig. 5e). Subsequently, the slope is stable (Fig. 5f). This sliding
206 process is accompanied by the sinking of the slope.

207 (4) Test 4

208 When the first rainfall lasts for 45 min, the soil on the left slope toe starts to slip. Muddy water
209 flows from the area of sliding soil. When the rainfall lasts for 78 min, the area of instability soil
210 extends to the slope shoulder. However, only a small amount of soil on the right slope toe slips.
211 During the second rainfall, the right slope is scoured away by rain, which results in a deep gully.
212 When the rainfall lasts for 496 min, the soil on the right side of slope slips, but the slide scale is small.
213 The slope is not completely destroyed.

214 (5) Test 5

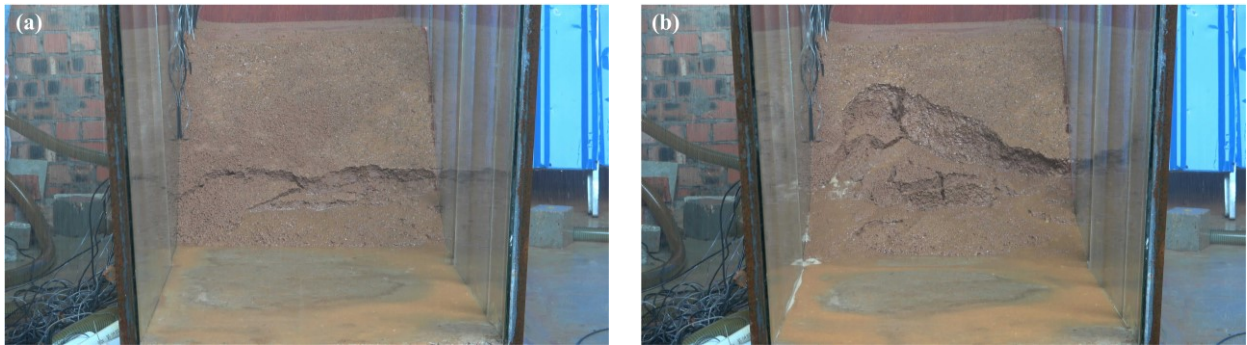
215 When the first rain lasts for 26 min, the soil on the right foot begins to slide. The failure range
216 extends to the middle of slope as the rainfall continues. At the same time, rainfall gravity leads to the
217 formation of low-lying areas. When the rainfall duration is 208 min, the sunken area becomes larger,
218 and the soil at the slope toe has basically slipped. When the second rainfall lasts for 766 min, the
219 low-lying areas are connected, and a steep free surface is formed. Subsequently, the soil at the slope

220 toe continues to slide. In the third rainfall, a small amount of soil slips. However, there is no
221 significant change in the slope eventually.

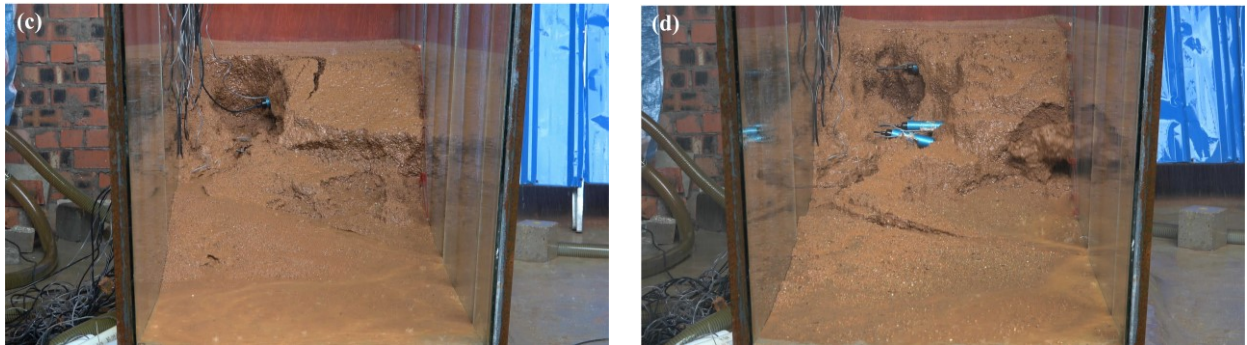
222 (6) Test 6

223 When the rainfall lasts for 5 min, tensile cracks occur at the slope toe, resulting in the soil failure.
224 When the rainfall lasts for 27 min, the failure range extends to the shoulder of slope. Subsequently,
225 massive soil on the free surface slides from time to time. When the rainfall lasts for 96 min, the soil
226 in the middle of slope begins to slip, causing the exposure of sensor #7. When the rainfall lasts for
227 133 min, the soil on the left slope shoulder begins to slide. The slope begins to be sinking. When the
228 rainfall lasts for 220 min, the soil on the right slope toe continues to slide. The failure area extends to
229 the middle of slope as the rainfall continues. At the end of the rainfall, the soil on the right slope
230 shoulder remains stable.

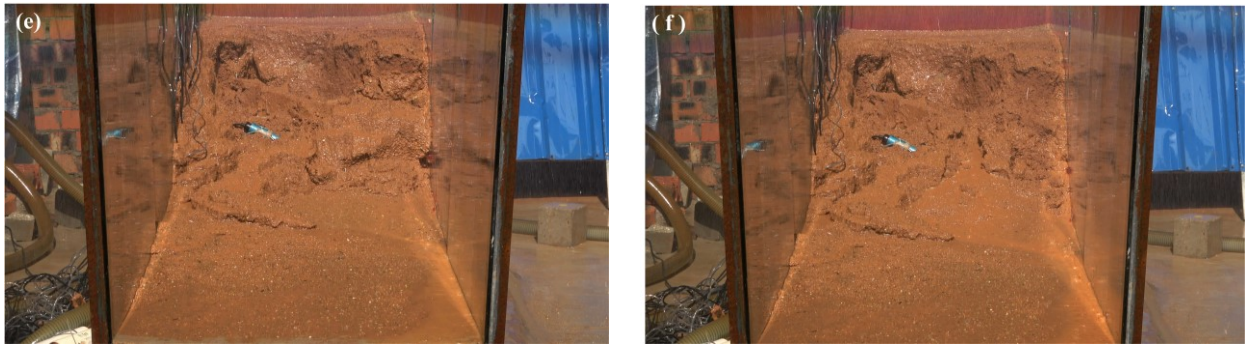
231



232



233



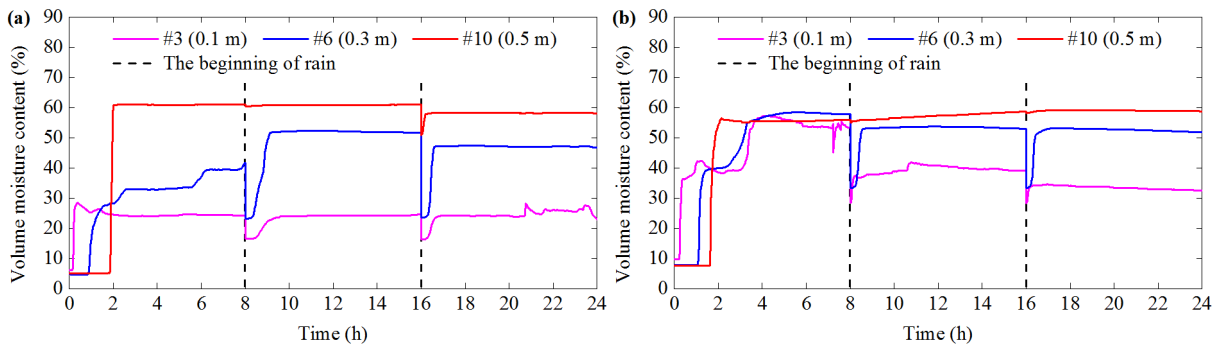
234 Figure 5. Typical phenomena of test 3. (a) The soil at the slope toe begins to slip after tensile cracks appear. (b) The soil
235 in the middle slope slides. (c) The soil on the slope shoulder slips owing to unbalance internal forces. (d) Blocky soil
236 slides suddenly on the right slope toe. (e) Massive soil on the right slope shoulder slides due to the unloading effect of the
237 slope toe. (f) The slope is stable at the end of the rainfall.

238 **3.2 Volume moisture content**

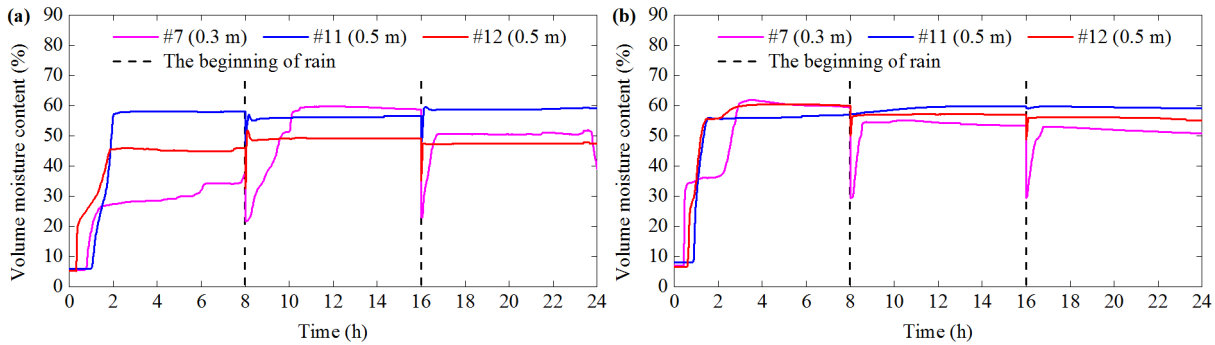
239 A-E inside the flume model represents the crest, shoulder, middle, and foot of the slope respectively.
240 The variation characteristics of the volume moisture content (VMC) at A, B, and C are relatively

241 similar. Therefore, the VMC of C is selected in the paper to indicate a general trend. In addition, the
 242 three positions (C, D, and E) are close to the sliding surface. Thus, the data of these three positions
 243 are analyzed in this section and shown in Figure 6-Figure 11. The general variation of VMC mainly
 244 consists of three stages: initial constant, significant increase, and stability. When the monitoring
 245 depth of the same position increases from 0.1 m to 0.5 m, the response time of VMC is delayed, and
 246 the stable VMC increases. It is attributed to the rainwater infiltration process and its accumulation. In
 247 addition, VMC is reduced due to water evaporation during the interval between two rainfall periods.
 248 This phenomenon is particularly obvious for soils with a depth of 0.1-0.3 m. VMC can be restored to
 249 the previous level or even higher value in subsequent rain.

250 Figure 6 and Figure 7 shows the differences of VMC between test 1 and test 2 as follows. (1)
 251 When the monitoring depth of the position C is 0.1 m and 0.3 m, the stable VMC of test 1 is smaller
 252 than that of test 2. The main reason is that the capacity of soil to store water can be enhanced as
 253 initial dry density (IDD) increases (Lu et al., 2018). (2) The VMC of three depths in the position C of
 254 test 2 is similar. However, the VMC between three depths of test 1 has great difference. It is
 255 especially noticeable in the first rain. (3) When the depth is 0.5 m, the VMC of the slope foot in test 1
 256 is significantly smaller than that of the slope middle, but the VMC at these two locations is similar in
 257 test 2.



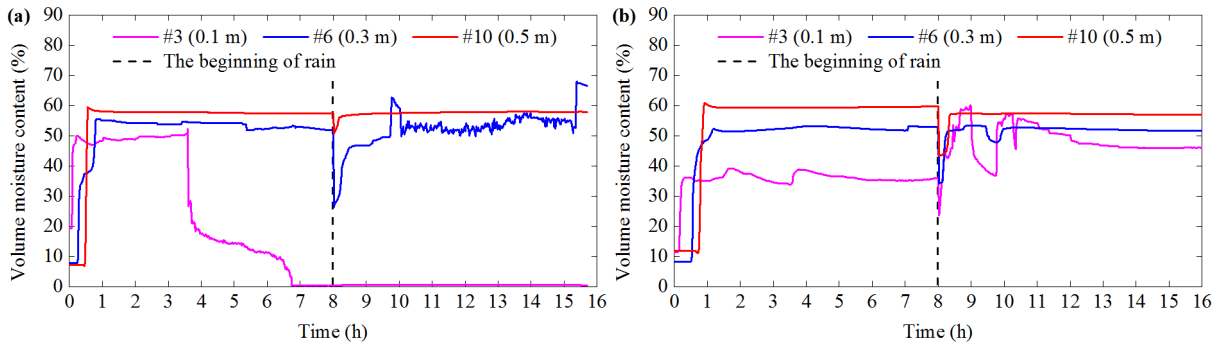
258
 259 Figure 6. Volume moisture content at position C of (a) test 1 and (b) test 2.



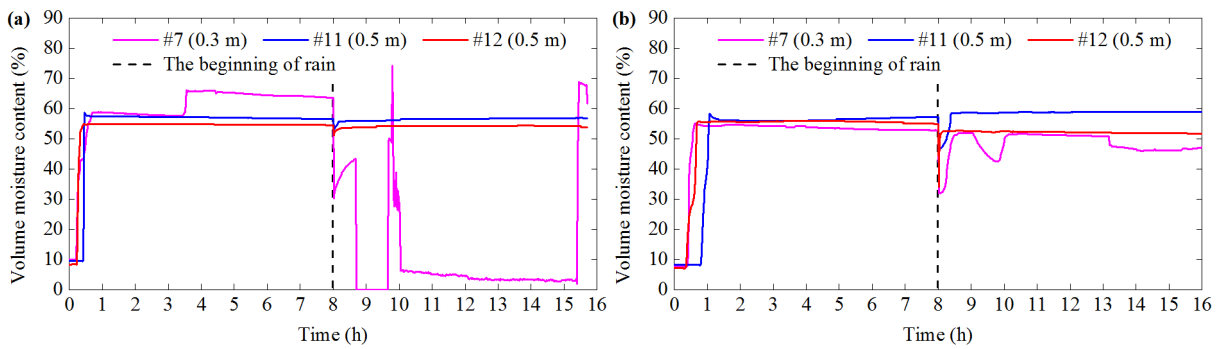
260
 261 Figure 7. Volume moisture content at position D and E of (a) test 1 and (b) test 2.

262
 263 The VMC of test 3 and test 4 is shown in Figure 8 and Figure 9. The response time of VMC of test
 264 3 is shorter than that of test 4 at the same location. The reason is that the increase of IDD results in
 265 the weakening of rain infiltration (Lee et al., 2005). The VMC at a depth of 0.1 m in test 3 decreases
 266 sharply and eventually becomes zero in the first rain (Fig. 8a). This is due to the soil sliding causing
 267 the third sensor to deviate from its original position. In addition, the VMC at the depth of 0.3 m in C
 268 and D of test 3 fluctuates significantly (Figs. 8a and 9a). The macroscopic phenomena in section 3.1

269 indicate that the time of the soil failure is basically corresponding to the fluctuation time. Thus, the
 270 fluctuation is attributed to the soil failure. The maintenance of water pipe causes a short water stop.
 271 Hence, VMC fluctuates at the beginning of the second rainfall in test 4 (Figs. 8b and 9b).

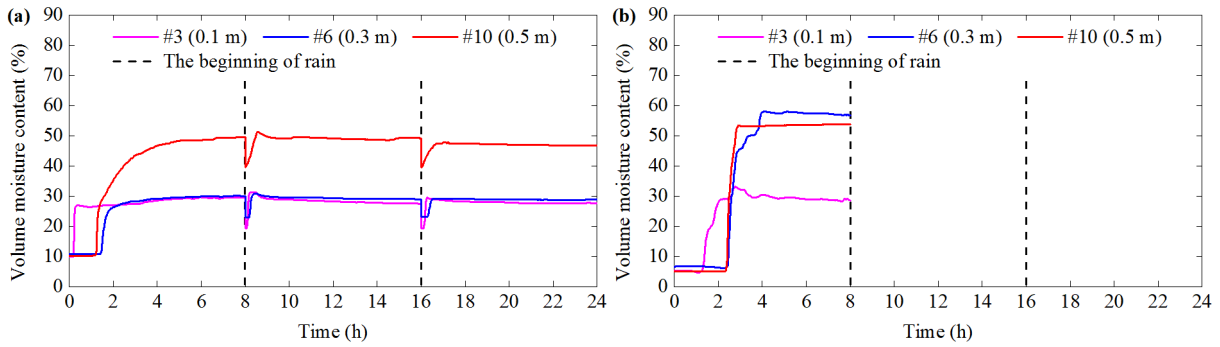


272
 273 Figure 8. Volume moisture content at position C of (a) test 3 and (b) test 4.



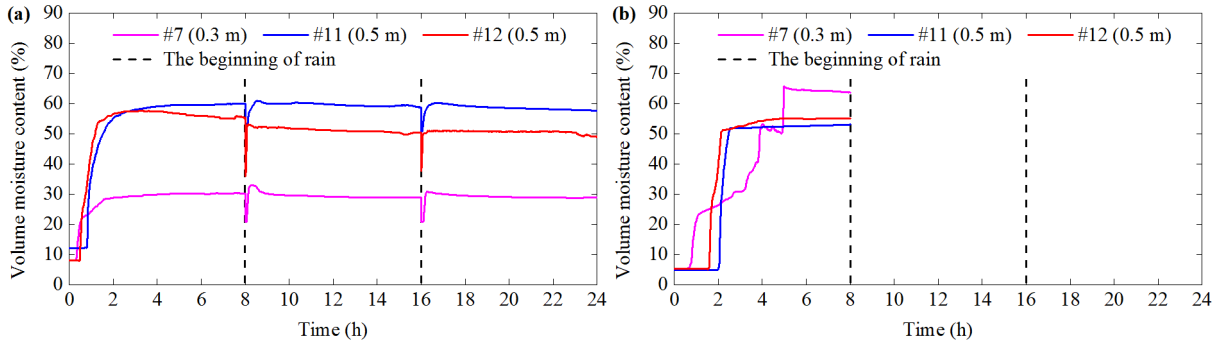
274
 275 Figure 9. Volume moisture content at position D and E of (a) test 3 and (b) test 4.

276
 277 The VMC of test 5 and test 6 is shown in Figure 10-Figure 11. When the rainfall intensity
 278 increases from 60 mm h^{-1} to 90 mm h^{-1} , the stable value of VMC of test 5 is less than that of test 6.
 279 However, the VMC in test 6 has a longer response time than that in test 5. It is obvious in the slope
 280 crest, such as the position C. The worth noting in section 3.1 is that the sliding time of test 6 is earlier
 281 than that in test 5. The main reasons of the above abnormal phenomena are including three aspects.
 282 One is that when the rainfall intensity is relative larger, more rainwater can penetrate the soil quickly.
 283 Shallow layer can be saturated rapidly. This process can cause silt and clay to migrate vertically and
 284 accumulate at a certain depth (Fang et al., 2012). Subsequently, the microstructure of soil is changed
 285 (Chen et al., 2018), and the infiltration path is blocked by the fine particles. Furthermore, rainwater
 286 cannot infiltrate the soil smoothly, and causes the long response time of VMC at the slope crest. The
 287 other is that rainfall infiltration can cause a difference in water pressure between the slope crest and
 288 the slope foot; this effect of seepage force will cause the slope foot to slide first (Zhou et al., 2014).
 289 In test 5 and test 6, the soil failures are both found in the slope foot at the beginning of rainfall. It is
 290 consistent with the research made by Zhou et al. (2014). This local deformation of the slope can
 291 cause internal force unbalance and soil microstructure change. The rainfall infiltration will be
 292 affected later (Chang et al., 2021). On the other hand, the tensile crack of the slope toe can provide a
 293 preferential path of rainwater. It is the main reason for the relative early sliding time in test 6.
 294 However, the sensor #12 cannot observe this data because it is not located under the crack.



295
296

Figure 10. Volume moisture content at position C of (a) test 5 and (b) test 6.

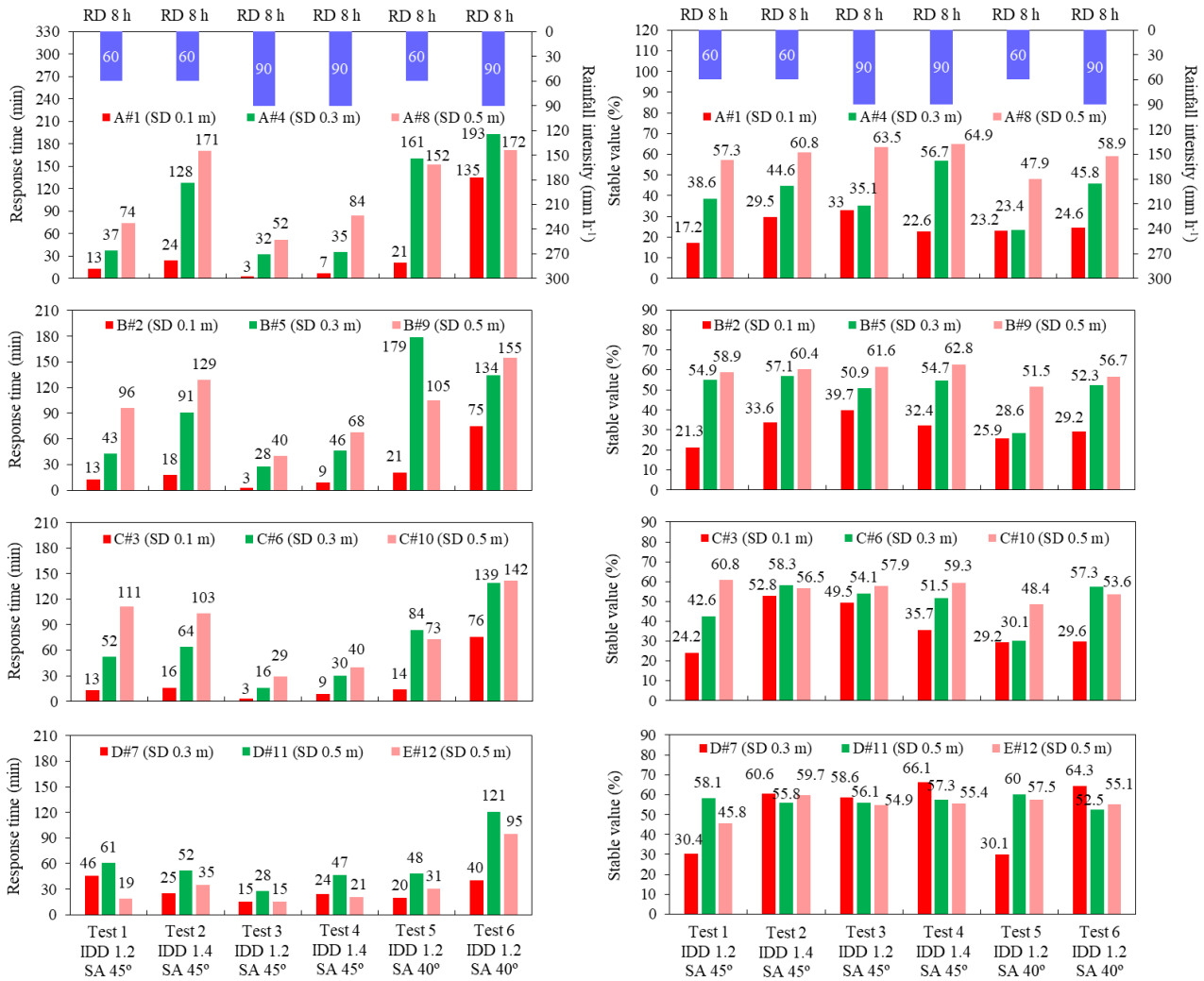


297
298
299

Figure 11. Volume moisture content at position D and E of (a) test 5 and (b) test 6.

300 Figure 12 shows the response time and stable VMC at five positions during the first rainfall. Test
301 1 and Test 2, Test 3 and Test 4 in Figure 12 are respectively compared. The similar result is that when
302 an IDD increases from 1.20 g cm^{-3} to 1.40 g cm^{-3} , the response time of VMC at the same location is
303 delayed. However, this similarity does not apply to the position D. The reason is that the local soil
304 sliding is found in the shallow layer in the position D of test 2. It can lead to the decrease in the part
305 of the soil thickness. Thus, the position D of test 2 affected by the rainfall is earlier than that of test 1.

306 The stable VMC with an IDD of 1.20 g cm^{-3} is smaller than that of 1.40 g cm^{-3} . It is suitable for
307 most of the depths of test 1 to test 4. The abnormal points include as follows: the depth of 0.5 m at C
308 and D of test 1 and test 2, the depth of 0.1 m at A, B and C and the depth of 0.3 m at C of test 3 and
309 test 4. This is due to the difference in soil – water action during rainfall. When rainfall intensity is 60 mm h^{-1} ,
310 all the rainwater can percolate through the soil with an IDD of 1.20 g cm^{-3} and 1.40 g cm^{-3} .
311 However, when rainfall intensity is 90 mm h^{-1} and an IDD is 1.40 g cm^{-3} , the rainwater seepage
312 capacity is less than 90 mm h^{-1} . Subsequently, rainwater cannot completely penetrate the soil and
313 surface runoff is formed. The slope is eroded by surface runoff; it can be found in the macroscopic
314 phenomena of test 4. Therefore, even if the rainfall intensity is 90 mm h^{-1} , the stable value of VMC is
315 relative small. In addition, test 5 and test 6 have the same initial dry density, but the response time
316 cannot decrease when the rainfall intensity is from 60 mm h^{-1} to 90 mm h^{-1} . The reasons are
317 mentioned in the previous paragraph.

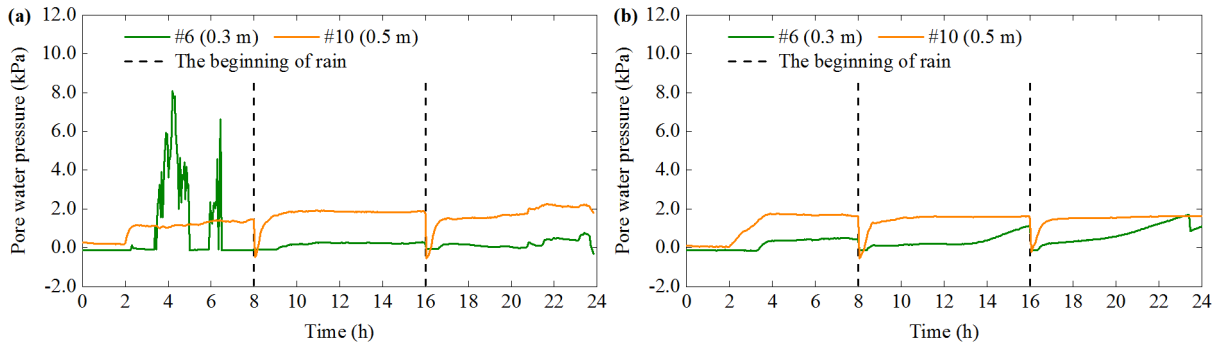


318

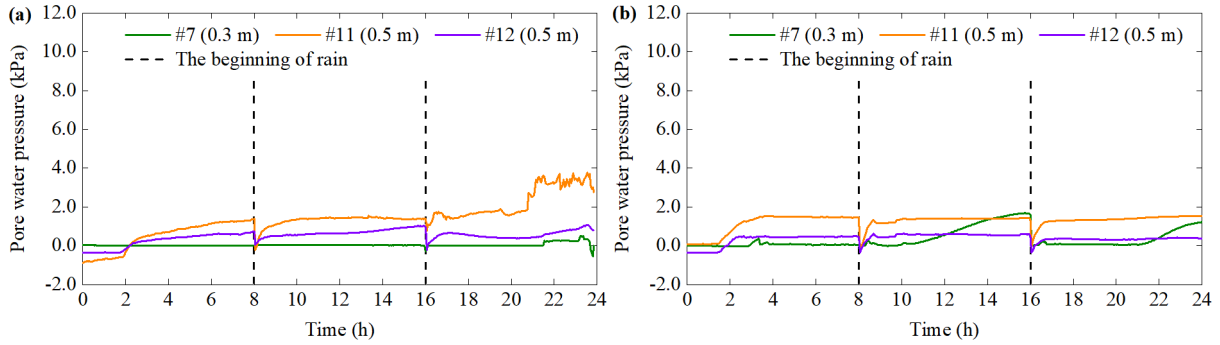
319 Figure 12. Response time and stable value of volume moisture content in six tests during the first rainfall. In this bar
 320 chart, IDD represents initial dry density, SA represents slope angle, SD represents sensor depth, and RD represents
 321 rainfall duration.

322 **3.3 Pore water pressure**

323 Pore water pressure (PWP) at three positions (C, D, E) is shown in Figure 13-Figure 18. The sensor
 324 #3 of PWP in test 2 and test 4 breaks down, and it deviates from its original position in test 3. Thus,
 325 the PMP of the sensor #3 are not analyzed in this section. The variation of PWP mainly consists of
 326 similar three parts: stability, significant increase, dynamic fluctuation. Some differences between
 327 these tests can be clarified. In test 1, the PWP at a depth of 0.3 m at C fluctuates drastically during
 328 the first rain. However, the PWP of test 2 does not fluctuate, and its variation is smaller than that in
 329 test 1 (Fig. 13). In addition, the PWP with a depth of 0.3 m at D varies gently in test 1, but it
 330 increases significantly during the second and third rain in test 2. The fluctuation occurs at a depth of
 331 0.5 m at D in test 1 (Fig. 14). The changes of PWP and VMC are not synchronized, which manifests
 332 in two aspects. One is the response time of PWP is later than that of VMC. The other is that VMC is
 333 in a stable stage when PWP fluctuates.

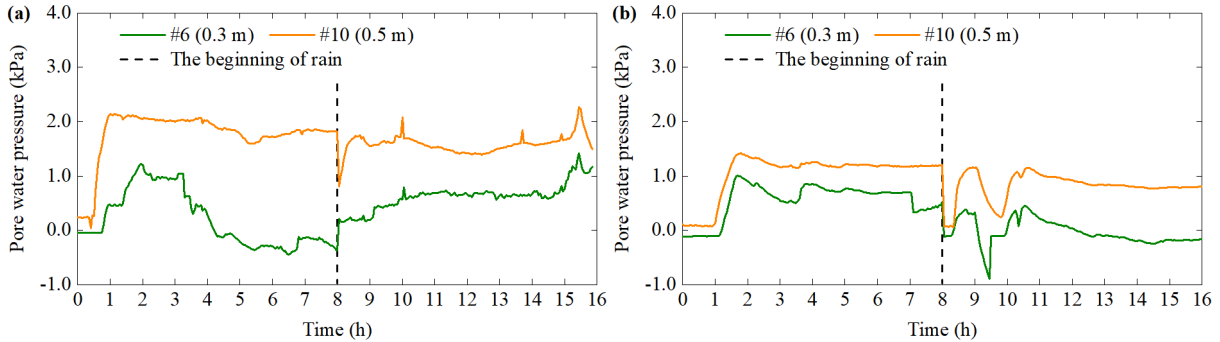


334
335 Figure 13. Pore water pressure at position C of (a) test 1 and (b) test 2.

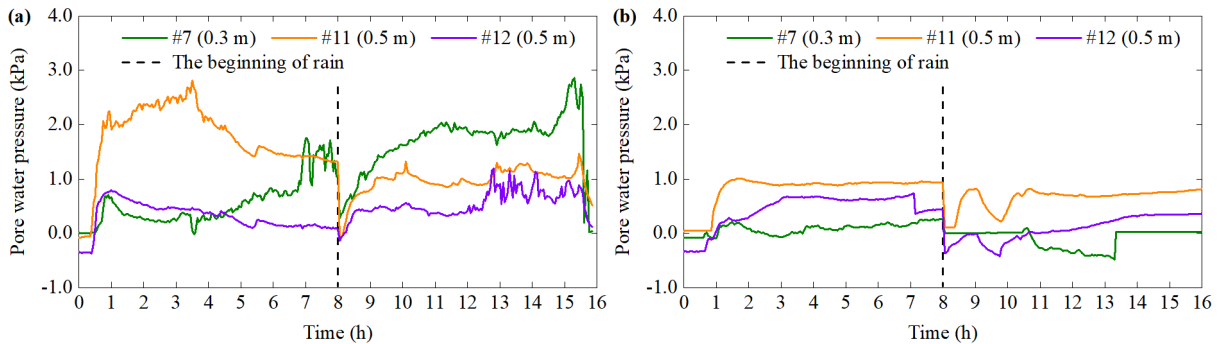


336
337 Figure 14. Pore water pressure at position D and E of (a) test 1 and (b) test 2.

338 In the first rainfall, the PWP response time of test 3 is shorter than that of test 4 at the same
339 location (Figs. 15 and 16). The difference in the response time is consistent with that in VMC. It
340 directly reflects the soil seepage capacity when an IDD is 1.20 g cm^{-3} and 1.40 g cm^{-3} respectively.
341 Besides, the frequent fluctuation of PWP mostly appears in test 3. In particular, the PWP in test 3 is
342 decreasing after increasing at the most locations except for the depth of 0.5 m of D. This downward
343 trend exists at position C of test 4, but is not significant at D and E.

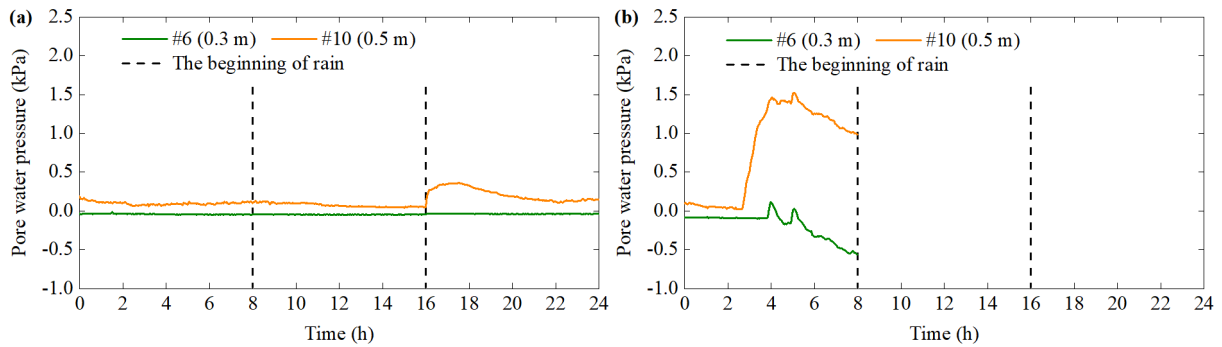


344
345 Figure 15. Pore water pressure at position C of (a) test 3 and (b) test 4.

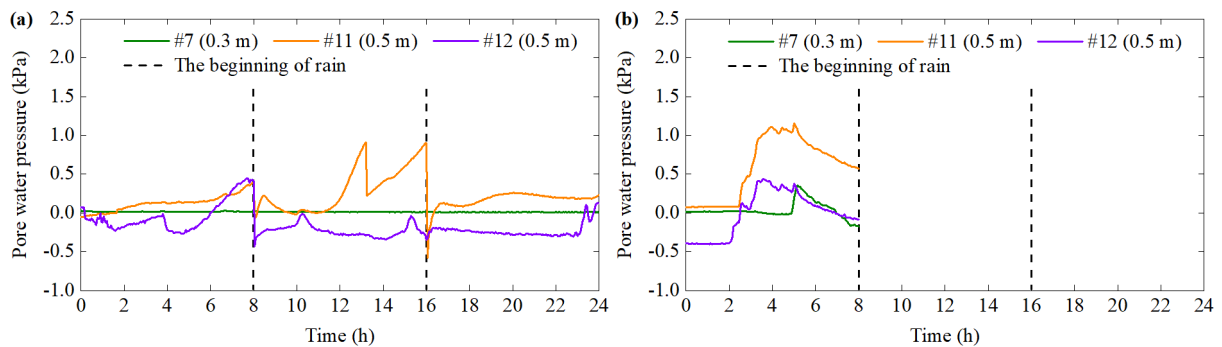


346
347 Figure 16. Pore water pressure at position D and E of (a) test 3 and (b) test 4.

348 Figure 17-Figure 18 shows the differences between test 5 and test 6 during the first rainfall. One is
 349 that the PWP curve at C in test 5 is flat. However, all the PWP in test 6 experiences the flat, increase
 350 and decrease stages. The other is that the PWP at E in test 5 has an obvious volatility characteristic. It
 351 fluctuates to the peak at the end of the first rain. Whereas, the PWP at E in test 6 has a downward
 352 trend after it reaches the peak. This opposite trend is related to the differences between the soil
 353 failures of these two tests. Soil sliding can cause stress to relax, which further results in an increase
 354 in soil porosity. It will induce pore water pressure to decrease. When rainwater is enough, pore water
 355 pressure can be restored.

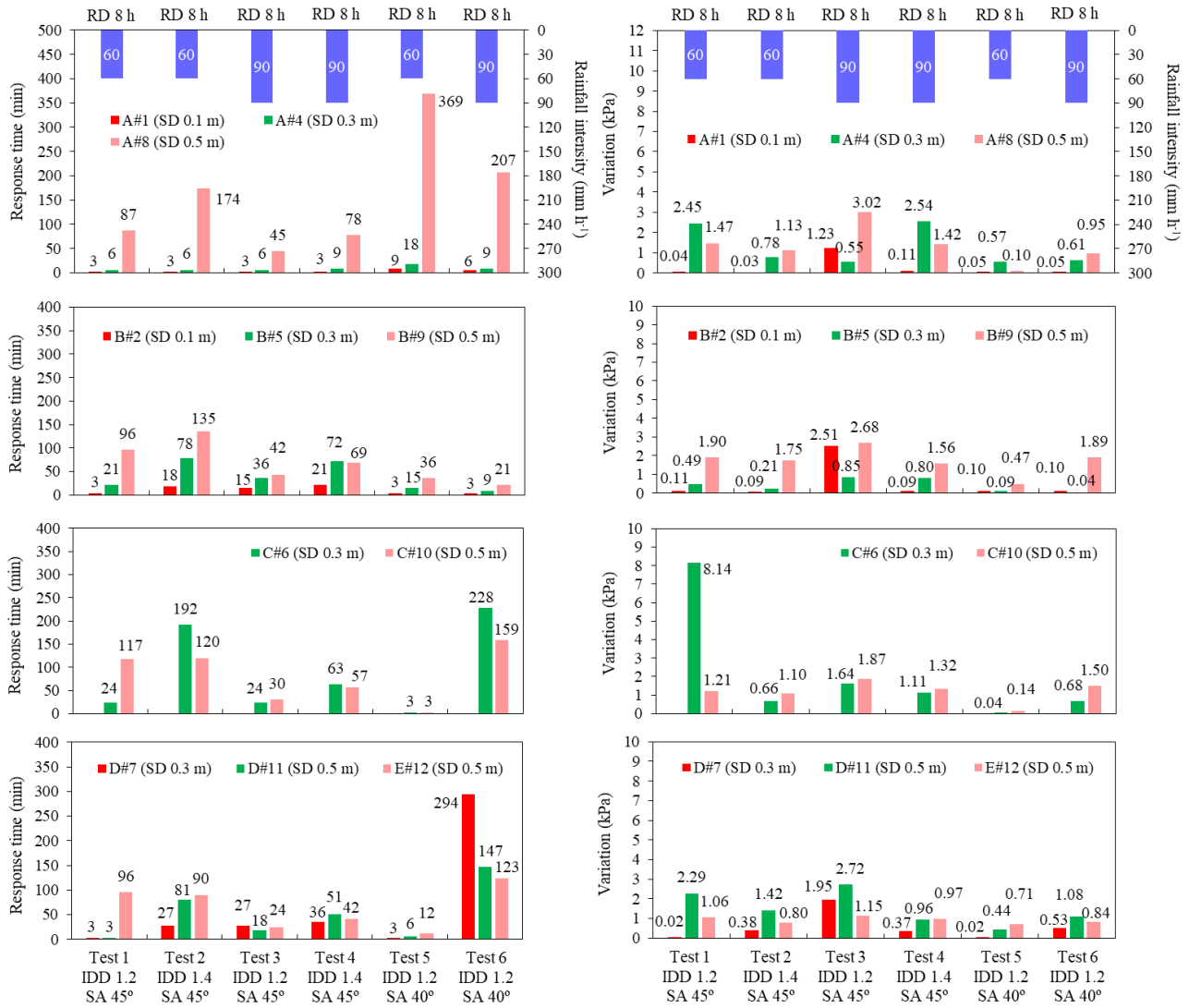


356
 357 Figure 17. Pore water pressure at position C of (a) test 5 and (b) test 6.



358
 359 Figure 18. Pore water pressure at position D and E of (a) test 5 and (b) test 6.

360 Figure 19 shows the response time and variation of PWP at five positions during the first rainfall.
 361 Test 1 and Test 2, Test 3 and Test 4 in Figure 19 are respectively compared. The main commonality is
 362 that when the location and rainfall duration is same, the response time of PWP with an IDD of 1.20 g cm^{-3}
 363 is shorter than that of 1.40 g cm^{-3} . Nonetheless, most of the variation in PWP has a contrary
 364 pattern. The reason is that even if the rainfall intensity is the same, the slope with different density
 365 has diverse hydrological characteristics (Lan et al., 2003). For example, slopes with high density
 366 have relatively low permeability and the change in PWP is limited. A significant difference is that
 367 although PWP change of the surface soil layer at each position is the smallest except for test 3, the
 368 PWP changes of other two depths do not increase with the increase of depth. The reasons are
 369 analyzed as follows. When the rainwater accumulates at a depth of 0.3 m, the PWP variation is
 370 relative large. At this moment, the PWP with a depth of 0.3 m can be larger than that of 0.5 m. The
 371 continuous seepage can cause soil gravity to increase. It can produce the compressive stress on the
 372 soil layer at a depth of 0.5 m. The further decrease in soil porosity can cause PWP to increase. At the
 373 same time, if the soil with a depth of 0.3 m begins to slide, PWP will be released. Therefore, in these
 374 conditions, the PWP with a depth of 0.5 m may be larger than that of 0.3 m. It suggests that changes
 375 in PWP depend on soil deformation and its diffusion. This validates the study by Iverson et al. (1997).



376

377 Figure 19. Response time and variation of pore water pressure in six tests during the first rainfall. In this bar chart, IDD
 378 represents initial dry density, SA represents slope angle, SD represents sensor depth, and RD represents rainfall duration.

379 **4 Discussion**

380 Six model tests have commonness in the patterns of slope failure based on the macroscopic
 381 phenomena. Based on these tests, the landslide formation can be classified into five stages and shown
 382 in Table 2. They are basically consistent with the results of the field survey in Southeast Guangxi
 383 (Wei et al., 2017). Therefore, the initiation processes of granite residual soil landslides can be
 384 reproduced by flume model tests.

385 (i) Rain infiltration and crack generation. At the beginning of rainfall, all rainwater can seep into
 386 the slope. There is no surface runoff on the slope. Volume moisture content begins to increase.
 387 However, matrix suction decreases, which results in the reduction of shear strength. In addition, the
 388 gravity load of the slope increases and favors the downward creep. The differential distribution of
 389 soil strength can cause cracks to generate at the slope toe, which provide a preferential path for
 390 rainwater.

391 (ii) Soil slide at the slope toe. As rainfall continues, rainwater penetrates the soil through the crack.
 392 The accumulated rainwater in the crack can produce the pressure acting on the slope. It facilitates the

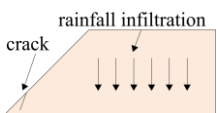
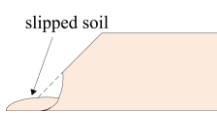
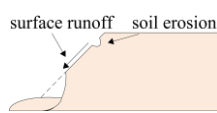
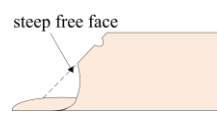
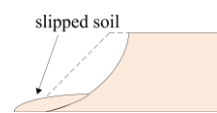





393 propagation of the crack. Hence, the soil strength around the crack decreases. Meanwhile, the
 394 underground runoff converges at the toe of the slope. The VMC at the slope toe is relative large. The
 395 water pressure's difference between the top and toe of the slope increases. This difference in pressure
 396 and changes in the soil microstructure can lead to a reduction in the shear strength of the slope.
 397 Therefore, the soil at the foot of the slope softens and slides first. Subsequently, muddy water
 398 gradually flows out from the slope toe. This indicates that fine particles migrate through subsurface
 399 runoff, causing changes in the microstructure of some soils along the flow network.

400 (iii) Occurrence of surface runoff and soil erosion. The water content of shallow soil layer
 401 increases to a saturation value with the continuing rain. A saturation zone appears. This process
 402 allows fine particles to migrate vertically to a certain depth. Subsequently, the infiltration path will be
 403 blocked, and rainwater cannot permeate the soil smoothly. The surface runoff gradually forms. On
 404 the other hand, the gravel of the soil remains on the slope surface, which is conducive to seepage
 405 along the slope. Therefore, subsurface runoff can lead to the loss of the surface layer soil. Multiple
 406 low-lying areas and ditches are generated by the erosion of surface runoff and splash erosion of
 407 rainfall. The erosion destruction is most serious in the slope toe and the slope middle.

408 (iv) Formation of steep-free surface. As the soil at the foot of the slope continues to slide, the
 409 geometry and stress of the slope have changed due to the removal of downward support. Even the
 410 internal force balance of the slope is destroyed. The unstable range expands to the surroundings. A
 411 steep free surface begins to form subsequently. However, the soil on the top of the slope has not
 412 slipped.

413 (v) Soil slide at the upper slope. The presence of macro-pores between the gravel can promote the
 414 rainwater penetration through the soil. This process facilitates the rainwater transmission to a deep
 415 layer. The sliding force of the slope can be further improved. Meanwhile, the unbalance internal
 416 forces gradually increase due to the repeat slide of the slope toe. Besides, the increase of PWP leads
 417 to a reduction in the effective stress and shearing strength. Finally, when the sliding force is greater
 418 than the soil resistance, the soil at the slope top begins to slide. Obvious shear deformation is formed.

419 Table 2. Schematic diagrams and photos of the landslide formation

Stage	Rain infiltration and crack generation	Soil slide at the slope toe	Occurrence of surface runoff and soil erosion	Formation of steep-free face	Soil slide at the upper slope
Schematic diagram					
Photo					

420
 421 One difference between six tests is the time of landslide initiation (Table 3). Six initiation times
 422 are 50 min, 67 min, 32 min, 45 min, 26 min and 5 min respectively. When the slope angle and
 423 rainfall intensity are the same, the initiation time of a landslide with a density of 1.20 g cm^{-3} is
 424 shorter than that of a landslide with a density of 1.40 g cm^{-3} . The difference is 17 min and 13 min.

425 The reason is that when the IDD increases, the slope permeability decreases (Lan et al., 2003), and
 426 the infiltration process is relative slow. Therefore, the slope needs more penetration time. This
 427 corresponds to the difference of the response time of VMC in section 3.2. In section 3.2, when an
 428 IDD increases from 1.20 g cm^{-3} to 1.40 g cm^{-3} , the response time of VMC and PWP is delayed. The
 429 decrease rate of the shearing strength is correspondingly slow. This is beneficial to the stability of the
 430 slope. When the slope angle and density are the same, the initiation time of a landslide with the
 431 rainfall intensity of 90 mm h^{-1} is 18 min-22 min shorter than that of a landslide with the rainfall
 432 intensity of 60 mm h^{-1} . The reason is that when the rainfall intensity is relative larger, more rainwater
 433 can penetrate the soil quickly. This leads to a rapid increase in VMC and PWP in shallow soil layers.
 434 The shearing strength decreases. At this time, the difference of water pressure between the slope toe
 435 and the slope crest is obvious, which result in the first soil sliding at the slope toe. Meanwhile, when
 436 the IDD is 1.20 g cm^{-3} , the rainfall intensity is 60 mm h^{-1} and 90 mm h^{-1} , if a slope angle increases
 437 from 40° to 45° , the starting time can be delayed by 24 min and 27 min. This is because steep slopes
 438 are not conducive to infiltration of rainwater (Xu et al., 2018). Hence, the VMC and PWP respond to
 439 rainfall slowly, which is favorable to slope stability. In a word, the initiation time of landslide is
 440 closely related to density, slope angle, and rainfall intensity. It is mainly controlled by the
 441 hydrological response of the slope.

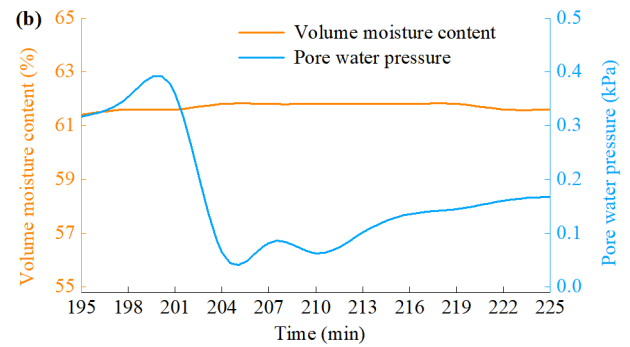
442 Table 3. Initiation time of landslide for six tests.

Test number	1	2	3	4	5	6
Initiation time (min)	50	67	32	45	26	5

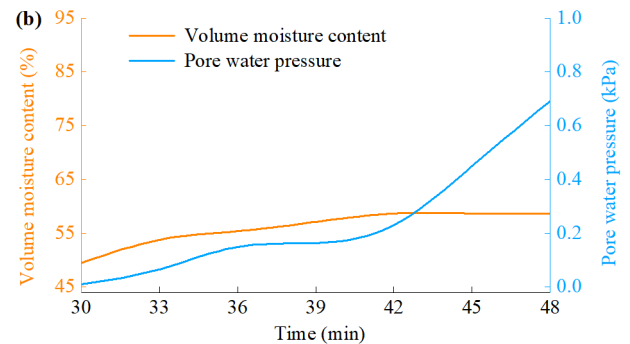
443
 444 The other difference in six tests is the failure mode and process of landslide. In test 1, all the
 445 surface soil slips, and the frequent sliding soil is in the shape of a block. In test 2, the sliding area
 446 slowly spreads to the surroundings, and the partial right shoulder fails to slide eventually. In test 3,
 447 the soil around the crack slides quickly, and all the soil on the slope surface is destroyed. In test 4, the
 448 scouring action of rain results in the formation of a deep gully, but the slope has stabilized finally. In
 449 test 5, the low-lying areas are enlarged with the continuous rainfall, and all the soil at the slope toe
 450 slips suddenly. In test 6, the soil surrounding crack slide rapidly, and the soil failure are repetitive.
 451 The above mentioned macroscopic phenomenon contains two main characteristics. When the IDD is
 452 1.20 g cm^{-3} , tensile crack is an important triggering factor for soil failure, and the formation process
 453 of landslide is relatively sudden and large in scale. When the IDD is 1.40 g cm^{-3} , the soil failure of
 454 the slope foot can trigger the trailing edge slip. Therefore, the sliding process is gradual and small-
 455 scale, often accompanied by the appearance of low-lying areas and ditches. The main reason is the
 456 energy required for the destruction of large density is significantly greater than that of small density
 457 (Xu et al., 2018). Hence, the formation process of landslide is different due to the initial state of the
 458 slope.

459 Section 3.3 shows that the pore water pressure fluctuates significantly during the soil failure.
 460 However, the variation of pore water pressure at the same position and depth is not synchronized
 461 with the water content. The typical periods of test 2 and the test 3 are selected in this section to
 462 understand the relationship between them. In test 2 with an IDD of 1.40 g cm^{-3} , when the rainfall
 463 lasts for 195 min-225 min, the soil in the slope middle slides. It promotes the development of cracks
 464 and causes massive soil to slide (Fig. 20a). The seventh sensor is the closest to unstable soil, thus, the

465 data of this sensor is selected for detailed analysis. Figure 20b shows that the water content is stable
 466 at about 61.6 % during this period, and the soil is in an over-saturated state. However, pore water
 467 pressure gradually increases to a peak of 0.361 kPa when the rainfall duration is 195 min-201 min.
 468 Subsequently, pore water pressure decreases rapidly, and maintains a certain degree of volatility.
 469 When the rainfall duration is 210 min, pore water pressure begins to increase again. In test 3 with an
 470 IDD of 1.20 g cm^{-3} , when the rainfall lasts for 30 min-48 min, the shallow soil is softened and slides
 471 many times (Fig. 21a). Figure 21b shows that when the rainfall duration is 30 min-36 min, VMC and
 472 PWP both increases; when the rainfall lasts for 36 min, the increasing trend of them is relatively
 473 gentle; when the rainfall lasts for 42 min, although PWP increases rapidly again, but VMC remains
 474 stable at 58.7 %. In a word, the differences in the variation of PWP and VMC comprise two aspects.
 475 One is that when VMC begins to increase, PWP is invariant. The response time of PWP is behind
 476 that of VMC. The other is that when VMC is constant or is in a significant rise, PWP has almost no
 477 change or only dramatic fluctuations. These may be related to mechanical behavior of granite
 478 residual soil.



479
 480 Figure 20. Typical phenomenon and result with an initial dry density of 1.40 g cm^{-3} . (a) Slope failure. (b) Results for
 481 sensor #7 closest to sliding surface.



482
 483 Figure 21. Typical phenomenon and result with an initial dry density of 1.20 g cm^{-3} . (a) Slope failure. (b) Results of
 484 sensor #7 closest to sliding surface.

485
 486 The above results may be explained by the research made by Iverson (Iverson, 2005; Iverson et al.,
 487 2000). He found that landslide mobilization was affected by the mechanical properties of shear bands
 488 that were related to the initial density. When dry density is low and rainfall intensity is high, the
 489 hammering effect of rain can squeeze the shallow soil. In addition, pore water pressure can increase
 490 due to the decrease in void ratio and leads to a reduction in shear strength. When the initial local
 491 shear deformation occurs, the shear zone is mainly contractive. Subsequently, excessive pore water
 492 pressure is generated. However, excess pore water pressure is difficult to dissipate completely in a

493 short time. This condition can promote the continuous increase of pore water pressure and the
494 connection of potential sliding surfaces. Therefore, the type of landslide failure is a sudden sliding
495 type in the macroscopic phenomenon (Dai et al., 1999a; Dai et al., 1999b; Mckenna et al., 2011).
496 When the dry density is larger, the infiltration rate of rainwater is smaller. At the same time, the
497 response time of water content and pore water pressure is delayed. In addition, the fluctuation of pore
498 water pressure is limited. As a result, the ability of the slope to resist seepage damage is improved
499 effectively. When dilative shear deformation appears, it can cause the dissipation of pore water
500 pressure, and even leads to the appearance of negative pore water pressure (Chen et al., 2018). It can
501 results in the delay of the VMC and the recovery of the shear strength. After that, long-term rainfall
502 can restore the loss of pore pressure due to soil dilation, and shear deformation will reappear. At this
503 time, the macroscopic phenomenon of landslide start is progressive (Dai et al., 1999a; Dai et al.,
504 1999b; Mckenna et al., 2011). The landslide mobilization mode in this paper is consistent with the
505 above mentioned.

506 Finally, the limitation of the model tests in this paper should be discussed. All sensors are
507 embedded in the center section of the slope (Fig. 4). Therefore, the sensors are less affected by the
508 left or right boundary. Monitoring data are reliable and can reflect the variation of VMC and PWP
509 during landslide formation. Because the sensor is connected to the data collector, the connecting line
510 is embedded in the slope. The surrounding soil is compacted to achieve the preset dry density.
511 However, the influence caused by the material heterogeneity of the connecting line, and the soil
512 cannot be eliminated. The effect is reflected in difference in rainwater infiltration. This may cause the
513 right side of the slope to tend to slide locally (Fig. 5 and Fig. 20). Nevertheless, this trend is
514 temporary and does not dominate the five similar stages of landslide formation. In addition, the five
515 stages are basically consistent with the field survey in Southeast Guangxi (Wei et al., 2017). In
516 conclusion, the model tests in this paper reproduce the failure pattern of granite residual soil slope
517 well. In future research, wireless transmission system will be employed to collect sensor data. This
518 can minimize the disturbance caused by the sensor line.

519 **5 Conclusion**

520 The present study is executed to analyze the failure mode and process of granite residual soil
521 landslides in Guangxi province, China. The following conclusions can be summarized.

522 (1) Volume moisture content and pore water pressure exhibits a non-synchronous response to the
523 rain. Initial dry density and rainfall intensity has a significant effect on the hydrological response.
524 Large density can restrain the rainwater infiltration rate and limit the fluctuation of pore water
525 pressure. In addition, high rainfall intensity is corresponding to the short response time of volume
526 moisture content. However, this is unsuitable for the soil with a small density, as changes in the soil
527 microstructure can alter the seepage path. The fluctuation of pore water pressure depends on soil
528 mechanical behavior and its diffusion.

529 (2) The differences in the formation process of granite residual soil landslides include the initiation
530 time and mode. The starting time of landslide is closely related to initial dry density, slope angle, and
531 rainfall intensity. It is mainly controlled by the hydrological response of the slope. The initiation time
532 of 1.20 g cm^{-3} is 13 min-17 min earlier than that of 1.40 g cm^{-3} . The initiation time of 90 mm h^{-1} is
533 18 min-22 min shorter than that of 60 mm h^{-1} . Mechanical properties of the shear zone play the
534 important role in the failure modes of landslides, which are closely related to the initial dry density.

535 Two failure modes can be observed. One is a sudden sliding in a large scale with a density of 1.2 g
536 cm⁻³; the other is a progressive sliding in a small scale with a density of 1.40 g cm⁻³.

537 (3) Landslide mobilization can be classified into five stages as follows: rain infiltration and crack
538 generation, soil slide at the slope toe, occurrence of surface runoff and soil erosion, formation of
539 steep-free surface, and soil slide at the upper slope. It is accompanied by the migration of fine
540 particles, and the formation of crack and macro-pores. Cracks and macro-pores can facilitate the
541 hydrological response in the deep layer.

542 Future research includes four aspects. Firstly, more tests involving multiple factors will be
543 conducted through the orthogonal experimental design. Secondly, triaxial instrument will be used to
544 perform the stress path tests. Thirdly, the influence of variation of initial dry density along the
545 vertical direction on slope failure will be analyzed. Fourthly, the quantitative relationship between
546 volume moisture content and pore water pressure during landslide initiation will be explored.

547

548 **Data availability**

549 All data in this study are available by contacting the first author: wushanbai@163.com.

550 **Author contributions**

551 SW carried out the artificial model tests, analyzed the experimental data, and wrote the manuscript.
552 RZ participated in the tests and analyzed part of the data. LL and YY guided the design and
553 implementation of the tests, as well as revised the content of the manuscript. YW and WW
554 participated in the implementation of the tests.

555 **Competing interests**

556 The authors declare that they have no conflict of interest.

557 **Acknowledgements**

558 This research was funded by the National Natural Science Foundation of China (Nos. 41901132,
559 51609041, 42261017), the Natural Scientific Project of Guangxi Zhuang Autonomous Region (Nos.
560 2021GXNSFBA220025, 2019GXNSFAA185015).

561

562 **References**

563 Calcaterra, D. and Parise, M.: Landslide types and their relationships with weathering in a Calabrian
564 basin, southern Italy, *B. Eng. Geol. Environ.*, 64, 193-207, <https://doi.org/10.1007/s10064-004-0262-5>, 2005.

566 Chang, Z., Huang, F., Huang, J., Jiang, S., Zhou, C., and Zhu, L.: Experimental study of the failure
567 mode and mechanism of loess fill slopes induced by rainfall, *Eng. Geol.*, 280, 1-16,
568 <https://doi.org/10.1016/j.enggeo.2020.105941>, 2021.

569 Chen, D. and Gong, X.: Experiment and modeling of soil-water characteristic curve of unsaturated
570 residual soil, *Rock and Soil Mechanics*, 35, 1885-1891, 2014 (in Chinese).

571 Chen, G., Meng, X., Qiao, L., Zhang, Y., and Wang, S.: Response of a loess landslide to rainfall:
572 observations from a field artificial rainfall experiment in Bailong River Basin, China, *Landslides*,
573 15, 895-911, <https://doi.org/10.1007/s10346-017-0924-6>, 2018.

574 Chen, H., Lee, C. F., and Law, K. T.: Causative mechanisms of rainfall-induced fill slope failures, *J.*

575 Geotech. Geoenviron. Eng., 130, 593-602, <https://doi.org/10.1061//asce/1090->
576 0241/2004/130:6/593, 2004.

577 Chen, N., Zhu, Y., Huang, Q., Iqbal, J., Deng, M., and He, N.: Mechanisms involved in triggering
578 debris flows within a cohesive gravel soil mass on a slope: a case in SW China, *J. Mt. Sci.*, 14,
579 611-620, <https://doi.org/10.1007/s11629-016-3882-x>, 2017.

580 Chen, X., Zhou, Q., and Cai, X.: Physical properties and shear strength characteristics of high liquid
581 limit granite residual soil, *Chinese Journal of Geotechnical Engineering*, 32, 901-908, 2011 (in
582 Chinese).

583 Coutinho, R. Q., Silva, M. M., dos Santos, A. N., and Lacerda, W. A.: Geotechnical characterization
584 and failure mechanism of landslide in granite residual soil, *J. Geotech. Geoenviron. Eng.*, 145, 1-
585 16, [https://doi.org/10.1061/\(asce\)gt.1943-5606.0002052](https://doi.org/10.1061/(asce)gt.1943-5606.0002052), 2019.

586 Dahal, R. K., Hasegawa, S., Nonomura, A., Yamanaka, M., Masuda, T., and Nishino, K.: Failure
587 characteristics of rainfall-induced shallow landslides in granitic terrains of Shikoku Island of Japan,
588 *Environ. Geol.*, 56, 1295-1310, <https://doi.org/10.1007/s00254-008-1228-x>, 2008.

589 Dai, F., Lee, C. F., and Wang, S.: Analysis of rainstorm-induced slide-debris flows on natural terrain
590 of Lantau Island, Hong Kong, *Eng. Geol.*, 51, 279-290, <https://doi.org/10.1016/s0013->
591 7952(98)00047-7, 1999a.

592 Dai, F., Lee, C. F., Wang, S., and Feng, Y.: Stress-strain behaviour of a loosely compacted volcanic-
593 derived soil and its significance to rainfall-induced fill slope failures, *Eng. Geol.*, 53, 359-370,
594 [https://doi.org/10.1016/s0013-7952\(99\)00016-2](https://doi.org/10.1016/s0013-7952(99)00016-2), 1999b.

595 Elkamhawy, E., Wang, H., Zhou, B., and Yang, Z.: Failure mechanism of a slope with a thin soft
596 band triggered by intensive rainfall, *Environ. Earth. Sci.*, 77, 340-354,
597 <https://doi.org/10.1007/s12665-018-7538-8>, 2018.

598 Fan, X., Juang, C., Wasowski, J., Huang, R., Xu, Q., Scaringi, G., van Westen, C., and Havenith, H.:
599 What we have learned from the 2008 Wenchuan Earthquake and its aftermath: A decade of
600 research and challenges, *Eng. Geol.*, 241, 25-32, <https://doi.org/10.1016/j.enggeo.2018.05.004>,
601 2018.

602 Fang, H., Cui, P., Pei, L., and Zhou, X.: Model testing on rainfall-induced landslide of loose soil in
603 Wenchuan earthquake region, *Nat. Hazard. Earth. Sys.*, 12, 527-533,
604 <https://doi.org/10.5194/nhess-12-527-2012>, 2012.

605 Fu, R., Hu, X., Zhou, B., Wang, H., and Wang, J.: A quantitative characterization method of 3D
606 morphology of sand particles, *Rock and Soil Mechanics*, 39, 483-490, 2018 (in Chinese).

607 Gasmol, J. M., Rahardjo, H., and Leong, E. C.: Infiltration effects on stability of a residual soil slope,
608 *Comput. Geotech.*, 26, 145-165, [https://doi.org/10.1016/s0266-352x\(99\)00035-x](https://doi.org/10.1016/s0266-352x(99)00035-x), 2000.

609 Huang, C.-C. and Yuin, S.-C.: Experimental investigation of rainfall criteria for shallow slope
610 failures, *Geomorphology*, 120, 326-338, <https://doi.org/10.1016/j.geomorph.2010.04.006>, 2010.

611 Huang, C.-C., Lo, C.-L., Jang, J.-S., and Hwu, L.-K.: Internal soil moisture response to rainfall-
612 induced slope failures and debris discharge, *Eng. Geol.*, 101, 134-145,
613 <https://doi.org/10.1016/j.enggeo.2008.04.009>, 2008.

614 Igwe, O. and Fukuoka, H.: The effect of water-saturation on the stability of problematic slopes at the
615 Iva Valley area, Southeast Nigeria, *Arab. J. Geosci.*, 8, 3223-3233,
616 <https://doi.org/10.1007/s12517-014-1398-7>, 2014.

617 Iverson, R. M.: Regulation of landslide motion by dilatancy and pore pressure feedback, *J. Geophys.*
618 *Res-Earth.*, 110, 1-16, <https://doi.org/10.1029/2004JF000268>, 2005.

619 Iverson, R. M., Reid, M. E., and LaHusen, R. G.: Debris-flow mobilization from landslides, *Annu.*
620 *Rev. Earth Pl. Sc.*, 25, 85-138, <https://doi.org/10.1146/annurev.earth.25.1.85>, 1997.

621 Iverson, R. M., Reid, M. E., Iverson, N. R., LaHusen, R. G., and Logan, M.: Acute sensitivity of
622 landslide rates to initial soil porosity, *Science*, 290, 513-516,
623 <https://doi.org/10.1126/science.290.5491.513>, 2000.

624 Jiang, Y., Chen, W., Wang, G., Sun, G., and Zhang, F.: Influence of initial dry density and water
625 content on the soil-water characteristic curve and suction stress of a reconstituted loess soil, *B.*
626 *Eng. Geol. Environ.*, 76, 1085-1095, <https://doi.org/10.1007/s10064-016-0899-x>, 2017.

627 Jiao, J., Wang, X., and Nandy, S.: Confined groundwater zone and slope instability in weathered
628 igneous rocks in Hong Kong, *Eng. Geol.*, 80, 71-92, <https://doi.org/10.1016/j.enggeo.2005.04.002>,
629 2005.

630 Kassim, A., Gofar, N., Lee, L. M., and Rahardjo, H.: Modeling of suction distributions in an
631 unsaturated heterogeneous residual soil slope, *Eng. Geol.*, 131-132, 70-82,
632 <https://doi.org/10.1016/j.enggeo.2012.02.005>, 2012.

633 Kim, J., Jeong, S., Park, S., and Sharma, J.: Influence of rainfall-induced wetting on the stability of
634 slopes in weathered soils, *Eng. Geol.*, 75, 251-262, <https://doi.org/10.1016/j.enggeo.2004.06.017>,
635 2004.

636 Kim, M. S., Onda, Y., Kim, J. K., and Kim, S. W.: Effect of topography and soil parameterisation
637 representing soil thicknesses on shallow landslide modelling, *Quatern. Int.*, 384, 91-106,
638 <https://doi.org/10.1016/j.quaint.2015.03.057>, 2015.

639 Lacerda, W. A.: Landslide initiation in saprolite and colluvium in southern Brazil: Field and
640 laboratory observations, *Geomorphology*, 87, 104-119,
641 <https://doi.org/10.1016/j.geomorph.2006.03.037>, 2007.

642 Lan, H., Zhou, C., Lee, C. F., Wang, S., and Wu, F.: Stability response analysis of rainfall landslide
643 under instantaneous pore water pressure: a case study of natural rainfall landslide in Hong Kong,
644 *Science in China Ser. E Technological Sciences*, 119-136, 2003 (in Chinese).

645 Lee, I.-M., Sung, S.-G., and Cho, G.-C.: Effect of stress state on the unsaturated shear strength of a
646 weathered granite, *Can. Geotech. J.*, 42, 624-631, <https://doi.org/10.1139/t04-091>, 2005.

647 Li, Z., Tang, L., and Sang, H.: 3-D micro-structure of the particle and water morphology of the
648 granite residual soil, *Acta Scientiarum Naturalium Universitatis Sunyatseni*, 56, 15-21, 2017 (in
649 Chinese).

650 Liang, H., He, S., Lei, X., Bi, Y., Liu, W., and Ouyang, C.: Dynamic process simulation of
651 construction solid waste (CSW) landfill landslide based on SPH considering dilatancy effects, *B.*
652 *Eng. Geol. Environ.*, 2, 1-15, <https://doi.org/10.1007/s10064-017-1129-x>, 2017.

653 Liao, L., Yang, Y., Yang, Z., Zhu, Y., Hu, J., and Zou, D. H. S.: Mechanical state of gravel soil in
654 mobilization of rainfall-induced landslides in the Wenchuan seismic area, Sichuan province, China,
655 *Earth Surf. Dynam.*, 6, 637-649, <https://doi.org/10.5194/esurf-6-637-2018>, 2018.

656 Liao, L., Zhu, Y., Zhao, Y., Wen, H., Yang, Y., Chen, L., Ma, S., and Xu, Y.: Landslide integrated
657 characteristics and susceptibility assessment in Rongxian county of Guangxi, China, *J. Mt. Sci.*, 16,
658 657-676, <https://doi.org/10.1007/s11629-017-4804-2>, 2019.

659 Liu, W., Song, X., Luo, J., and Hu, L.: The processes and mechanisms of collapsing erosion for
660 granite residual soil in southern China, *J. Soil. Sediment.*, 20, 992-1002,
661 <https://doi.org/10.1007/s11368-019-02467-4>, 2020a.

662 Liu, W., Ouyang, G., Luo, X., Luo, J., Hu, L., and Fu, M.: Moisture content, pore-water pressure and
663 wetting front in granite residual soil during collapsing erosion with varying slope angle,
664 *Geomorphology*, 362, 1-10, <https://doi.org/10.1016/j.geomorph.2020.107210>, 2020b.

665 Liu, X., Zhang, X., Kong, L., Li, X., and Wang, G.: Effect of cementation on the small-strain
666 stiffness of granite residual soil, *Soils. Found.*, 61, 520-532,
667 <https://doi.org/10.1016/j.sandf.2021.02.001>, 2021.

668 Lu, Y., Wei, C., Cai, G., and Zhao, C.: Water-holding characteristics of weathered granite soils,
669 *Chinese Journal of Geotechnical Engineering*, 40, 96-100, 2018 (in Chinese).

670 Luo, X., Gao, H., He, P., and Liu, W.: Experimental investigation of dry density, initial moisture
671 content, and temperature for granite residual soil disintegration, *Arab. J. Geosci.*, 14, 1-9,
672 <https://doi.org/10.1007/s12517-021-07239-4>, 2021.

673 McKenna, J. P., Santi, P. M., Amblard, X., and Negri, J.: Effects of soil-engineering properties on
674 the failure mode of shallow landslides, *Landslides*, 9, 215-228, <https://doi.org/10.1007/s10346-011-0295-3>, 2011.

676 Miao, F., Wu, Y., Torok, A., Li, L., and Xue, Y.: Centrifugal model test on a riverine landslide in the
677 Three Gorges Reservoir induced by rainfall and water level fluctuation, *Geosci. Front.*, 13, 1-14,
678 <https://doi.org/10.1016/j.gsf.2022.101378>, 2022.

679 Ministry of Construction of the People's Republic of China: Code for investigation of geotechnical
680 engineering (GB50021-2001), China Architecture & Building Press, Beijing, 2002 (in Chinese).

681 Moriwaki, H., Inokuchi, T., Hattanji, T., Sassa, K., Ochiai, H., and Wang, G.: Failure processes in a
682 full-scale landslide experiment using a rainfall simulator, *Landslides*, 277-287,
683 <https://doi.org/10.1007/s10346-004-0034-0>, 2004.

684 Mukhlisin, M. and Taha, M. R.: Numerical model of antecedent rainfall effect on slope stability at a
685 hillslope of weathered granitic soil formation, *J. Geol. Soc. India.*, 79, 525-531,
686 <https://doi.org/10.1007/s12594-012-0077-0>, 2012.

687 Mukhlisin, M., Taha, M. R., and Kosugi, K.: Numerical analysis of effective soil porosity and soil
688 thickness effects on slope stability at a hillslope of weathered granitic soil formation, *Geosci. J.*, 12,
689 401-410, <https://doi.org/10.1007/s12303-008-0039-0>, 2008.

690 Ng, C. W. and Pang, Y. W.: Experimental investigations of the soil-water characteristics of a
691 volcanic soil, *Can. Geotech. J.*, 37, 1252-1264, <https://doi.org/10.1139/t00-056>, 2000.

692 Pham, K., Kim, D., Lee, I.-M., and Choi, H.: Hydraulic-mechanical properties of unsaturated granite-
693 weathered residual soil in Korea, *Vadose. Zone. J.*, 18, 1-13,
694 <https://doi.org/10.2136/vzj2018.10.0188>, 2019.

695 Qu, Y., Ng, C. W., and Shang, Y.: Study on latitudinal effect on lateritization of eluvial soil on
696 granite and cause for weak lateritization of the soil in Hong Kong, *Journal of Engineering Geology*,
697 16-20, 2000 (in Chinese).

698 Rahardjo, H., Leong, E. C., and Rezaur, R. B.: Effect of antecedent rainfall on pore-water pressure
699 distribution characteristics in residual soil slopes under tropical rainfall, *Hydrol. Process.*, 22, 506-
700 523, <https://doi.org/10.1002/hyp.6880>, 2008.

701 Rahardjo, H., Aung, K. K., Leong, E. C., and Rezaur, R. B.: Effects of pore-size distribution on
702 engineering properties of residual soils, in: Proceedings of the Second World Engineering
703 Congress, Geotechnical Engineering & Transportation, Sarawak, Malaysia, 22-25 July 2002, 70-
704 76, 2002.

705 Rahardjo, H., Lee, T. T., Leong, E. C., and Rezaur, R. B.: Response of a residual soil slope to rainfall,
706 *Can. Geotech. J.*, 42, 340-351, <https://doi.org/10.1139/t04-101>, 2005.

707 Rahardjo, H., Satyanaga, A., Leong, E.-C., Ng, Y. S., and Pang, H. T. C.: Variability of residual soil
708 properties, *Eng. Geol.*, 141-142, 124-140, <https://doi.org/10.1016/j.enggeo.2012.05.009>, 2012.

709 Rahman, A. S. A., Noor, M. J. M., Jais, I. B. M., Sidek, N., and Ahmad, J.: Shear strength of granitic
710 residual soil in saturated and unsaturated conditions, in: AIP Conference Proceedings, Advances in
711 Civil Engineering and Science Technology, Penang, Malaysia, 5-6 September 2018, 1-9, 2018.

712 Rezaur, R. B., Rahardjo, H., Leong, E. C., and Lee, T. T.: Hydrologic behavior of residual soil slopes
713 in Singapore, *J. Hydrol. Eng.*, 8, 133-144, [https://doi.org/10.1061/\(asce\)1084-0699\(2003\)8:3\(133\)](https://doi.org/10.1061/(asce)1084-0699(2003)8:3(133)),
714 2003.

715 Shu, R., Kong, L., Liu, B., and Wang, J.: Stress-strain strength characteristics of undisturbed granite
716 residual soil considering different patterns of variation of mean effective stress, *Appl. Sci-Basel.*,
717 11, 1-16, <https://doi.org/10.3390/app11041874>, 2021.

718 Take, W. A., Bolton, M. D., Wong, P. C. P., and Yeung, F. J.: Evaluation of landslide triggering
719 mechanisms in model fill slopes, *Landslides*, 1, 173-184, <https://doi.org/10.1007/s10346-004-0025-1>, 2004.

721 Tu, X. B., Kwong, A. K. L., Dai, F. C., Tham, L. G., and Min, H.: Field monitoring of rainfall
722 infiltration in a loess slope and analysis of failure mechanism of rainfall-induced landslides, *Eng.*
723 *Geol.*, 105, 134-150, <https://doi.org/10.1016/j.enggeo.2008.11.011>, 2009.

724 Wang, G. and Sassa, K.: Factors affecting rainfall-induced flowslides in laboratory flume tests,
725 *Geotechnique*, 51, 587-599, <https://doi.org/10.1680/geot.51.7.587.51386>, 2001.

726 Wang, Z., Mai, T., and Qi, C.: Shear strength and microstructure of compacted granite residual soils
727 in Rong County, *Hydrogeology & Engineering Geology*, 45, 101-107, 2018 (in Chinese).

728 Wei, C., Wen, H., Liao, L., Yang, Y., Ma, S., Zhao, Y., and Chen, L.: Failure characteristics and
729 prevention measures of granite residual soil slope in the southeast of Guangxi Province, China,
730 *Earth and Environment*, 45, 576-586, 2017 (in Chinese).

731 Wen, H.: A detailed survey report of geological disasters in Rongxian County, Guangxi., Guangxi
732 Zhuang Autonomous Region Geological Environmental Monitoring Station, Guilin, Guangxi., 196
733 pp., 2015 (in Chinese).

734 Wu, N.: Engineering characteristics of cutting slope of granite residual soil, *Mountain Research*, 24,
735 431-436, 2006a (in Chinese).

736 Wu, N.: Study on classification of granite residual soils, *Rock and Soil Mechanics*, 27, 2299-2304,
737 2006b (in Chinese).

738 Wu, Q., Tang, H., Ma, X., Wu, Y., Hu, X., Wang, L., Criss, R., Yuan, Y., and Xu, Y.: Identification
739 of movement characteristics and causal factors of the Shuping landslide based on monitored
740 displacements, *B. Eng. Geol. Environ.*, 78, 2093-2106, <https://doi.org/10.1007/s10064-018-1237-2>,
741 2019.

742 Xia, J., Cai, C., Wei, Y., and Wu, X.: Granite residual soil properties in collapsing gullies of south

743 China: spatial variations and effects on collapsing gully erosion, *Catena*, 174, 469-477,
744 <https://doi.org/10.1016/j.catena.2018.11.015>, 2019.

745 Xu, X. and Jian, W.: Experiment study on rainfall infiltration of slope under thrust at front end, *Rock*
746 *and Soil Mechanics*, 38, 3547-3554, 2017 (in Chinese).

747 Xu, X., Jian, W., and Wu, N.: Influence of repeated wetting cycles on shear properties of natural
748 residual soil *China J. Highw. Transp.*, 30, 33-40, 2017 (in Chinese).

749 Xu, X., Jian, W., Wu, N., Xu, X., and Liu, J.: Unsaturated seepage characteristics of slope under
750 rainfall infiltration, *Earth Science*, 43, 922-932, 2018 (in Chinese).

751 Yao, Y., Ni, J., and Li, J.: Stress-dependent water retention of granite residual soil and its
752 implications for ground settlement, *Comput. Geotech.*, 129, 1-11,
753 <https://doi.org/10.1016/j.compgeo.2020.103835>, 2021.

754 Zhai, Q., Rahardjo, H., and Satyanaga, A.: Variability in unsaturated hydraulic properties of residual
755 soil in Singapore, *Eng. Geol.*, 209, 21-29, <https://doi.org/10.1016/j.enggeo.2016.04.034>, 2016.

756 Zhan, L., Li, H., Chen, Y., and Fredlund, D. G.: Parametric analyses of intensity-duration curve for
757 predicting rainfall-induced landslides in residual soil slope in Southeastern coastal areas of China,
758 *Rock and Soil Mechanics*, 33, 872-880+886, 2012 (in Chinese).

759 Zhang, S. and Tang, H.: Experiment study of disintegration mechanism for unsaturated granite
760 residual soil, *Rock and Soil Mechanics*, 34, 1668-1674, 2013 (in Chinese).

761 Zhang, W. G., Zhang, R. H., Han, L., and Goh, A. T. C.: Engineering properties of the Bukit Timah
762 Granitic residual soil in Singapore, *Underground Space*, 4, 98-108,
763 <https://doi.org/10.1016/j.undsp.2018.07.001>, 2019.

764 Zhao, X. and Hu, H.: Investigation on failure of granitic residual slope by using centrifugal model
765 test, *Journal of Engineering Geology*, 13, 410-414, 2005 (in Chinese).

766 Zhao, Y., Sun, X., Wen, T., Chen, R., and Huang, L.: Micro-structural evolution of granite residual
767 soil under external loading based on X-ray micro-computed tomography, *Ksce. J. Civ. Eng.*, 25,
768 2836-2846, <https://doi.org/10.1007/s12205-021-0803-5>, 2021.

769 Zhou, J., Du, Q., Li, Y., and Zhang, J.: Centrifugal model tests on formation mechanism of landslide-
770 type debris flows of cohesiveless soils, *Chinese Journal of Geotechnical Engineering*, 36, 2010-
771 2017, 2014 (in Chinese).

772 Zhu, J.-H. and Anderson, S. A.: Determination of shear strength of Hawaiian residual soil subjected
773 to rainfall-induced landslides, *Geotechnique*, 48, 73-82, <https://doi.org/10.1680/geot.1998.48.1.73>,
774 1998.

775 Zuo, C., Xu, Y., Ding, S., and Tang, X.: Class soil landslide stability and its influencing factor
776 interaction law, *Research of Soil and Water Conservation*, 22, 325-330, 2015 (in Chinese).

777 Zou, Z., Yan, J., Tang, H., Wang, S., Xiong, C., and Hu, X.: A shear constitutive model for describing
778 the full process of the deformation and failure of slip zone soil, *Eng. Geol.*, 276, 1-11,
779 <https://doi.org/10.1016/j.enggeo.2020.105766>, 2020.